Vol. 2 June, 1958 No. 4

MINERALOGICAL JOURNAL

CONTENTS

X-Ray Power Patterns and Cell Dimensions of Some Chlorites in Japan, with a Note on Their Interference Colors ..... H. Shirozu 209

A Study on Monazite from the Ebisu Mine, Gifu Prefecture ..... T. Kato 224

Mineralogical Study on Some Pyrophyllites in Japan ..... H. Kodama 236

Infrared Absorption and Structures of Borate Polyatomic Ions ..... Y. Takéuchi 245

Elliptic Vibration of Light in Some Alkali Amphiboles ..... T. Shoda 269

Abstract of the Kobutsugaku Zasshi, Journal of the Mineralogical Society of Japan, Vol. 3, No. 5 279

The Mineralogical Society of Japan
Department of Geology and Mineralogy, Faculty of Science,
Hokkaido University, Sapporo, Japan

MINERALOGICAL JOURNAL

published by

The Mineralogical Society of Japan

EDITORIAL BOARD

Zyunpéi Harada, *Hokkaido University;* Teiichi Ito, *University of Tokyo;* (Chief) Nobuo Katayama, *University of Tokyo;* Keiichi Omori, *Tohoku University;* Ryôiti Kiriyama, *University of Osaka;* Seitaro Tsuboi, *University of Tokyo;* Takeo Watanabe, *University of Tokyo;* Toyofumi Yoshimura, *Kyushu University.*

Instructions to Contributors

Manuscripts of articles should be submitted to the executive editor, Nobuo Katayama, at the College of General Education, University of Tokyo, Komaba, Meguro-ku, Tokyo. The manuscript should be typewritten with double space lines, and not exceed 20 sheets of normal typewriting paper. References of literature should be in accordance with the forms used in the pages of this journal.

Plates and figures should be capable of reduction to not more than 10 by 15 centimetres. Line drawings should be in black India ink on white drawing board, tracing paper, or coordinate paper printed in blue. Photographs should be positive glossy prints.

Two referees chosen by the Editorial Board read the manuscript of article submitted before it is accepted for publication.

Thirty reprints without cover will be furnished to the author free of cost and without previous notice from him. Additional reprints will be furnished at cost when ordered.

The price of the journal to subscribers in Japan is 250 yen for a single copy (including postage), and to subscribers in other countries $ 1.00 (including postage) for a single copy, or $ 5.00 (including postage) per volume of 6 numbers.

Printed in Japan

MINERALOGICAL JOURNAL VOL. 2, NO. 4, PP. 209-223, JUNE, 1958

X-RAY POWDER PATTERNS AND CELL DIMENSIONS OF SOME CHLORITES IN JAPAN, WITH A NOTE ON THEIR INTERFERENCE COLORS

HARUO SHIROZU

Department of Geology, Faculty of Science, Kyushu University

ABSTRACT

X-ray powder studies on about fifty specimens of rather highly crystalline chlorites from Japan revealed the exsistence of two type of elementary cells, one with a 14Å-monoclinic and the other with a 14Å-ortho-hexagonal symmetry, and that the patterns of the former type are closely similar to one another, but those of the latter type vary from one another in detail. The monoclinic type ranges from Mg-rich chlorite to Fe-chlorite while the ortho-hexagonal type appears to be limited to Fe-rich members, but a Mg-rich specimen seems to have the latter type cell. The interference colors of the monoclinic types are frequently abnormal (usually for Fe-chlorite), the ortho-hexagonal types, however, usually show normal interference color, so that these two types are generally distinguishable under the microscope.

The results of chemical analyses and cell dimension determinations for the selected eleven chlorite specimens show that, as previously known, the basal spacing depends on the number of tetrahedral Al ions, and the *b* dimension on Fe atoms in the structure; these relations are not only more definitely established than in previous data but also suggest that both the basal spacings and the tetrahedral Al^{+3} ions of chlorite and/or serpentine can be dealt with in the same manner.

The estimation of the chemical composition of chlorites by X-ray method is also presented.

Introduction

Numerous X-ray powder data for chlorites, whose structure being of alternation of talc-like layer and brucite-like layer, are previously reported. A great many of them are essentially identical with those (monoclinic) by McMurchy[13], which are termed "normal chlorite type" by F. A. Bannister[10], but some of them are difficult to index[1)5)], and a

few are interpreted as having ortho-hexagonal cell[8)21)]; these are not yet systematized. The relations of the cell dimensions to chemical composition of chlorite are gradually being established[13)8)1)5)14)11)7)], but are not yet sufficient for estimating the chemical composition.

This paper is a preliminary report mainly concerning these problems for some chlorites in Japan.

Most of the specimens are well crystallized chlorites, which were collected by many workers as well as myself from various metal mines, crystalline schists, serpentines, igneous rocks, etc, in Japan. Fine-grained or poorly crystalline chlorite minerals found in the altered zone around ore deposits, the altered igneous rocks, the sedimentary rocks, etc. are not treated here.

Chemical composition

Pure and fresh eleven specimens, ranging from Mg-rich to Fe-rich are selected from the great many chlorite specimens and analyzed chemically and their atomic ratios are calculated on the basis of fourteen oxygen atoms (Table 1). The results agree closely to an ideal chlorite formula of Tschermak's "orthochlorite", $[(Mg, Fe^{2+})_{6-n}(Fe^{3+}, Al)_n][Al_nSi_{4-n}]O_{10}(OH)_8$.

X-ray powder pattern

General

X-ray powder patterns of rather highly crystalline chlorites with various chemical compositions show that the data of about forty specimens agree with those of well known chlorites (1-layer monoclinic type), and that those of several Fe-rich chlorites are interpreted for most lines in terms of an ortho-hexagonal elementary cell. The patterns of a few chlorites can be interpreted as those of a mixture of these two types. Some of these data for filtered Fe radiation, obtained with a 114.6 mm. diameter camera, are listed in Tables 2, 3 and 4. The two types are also optically distinct from each other from their interference colors as mentioned later.

Table 1. Chemical compositions of chlorites

(analyst, H. Shirozu)

No.	1	2	3	4	5
SiO_2	29.26	28.40	29.71	32.27	29.89
Al_2O_3	22.06	22.86	19.75	14.99	19.64
Fe_2O_3	1.05	0.27	0.29	1.56	0.61
FeO	none	3.01	6.59	6.89	9.23
MnO	0.69	0.21	0.30	0.09	0.09
MgO	34.08	32.08	30.79	31.75	29.38
CaO	none	—	tr.	tr.	tr.
H_2O^+	13.11	12.89	12.55	12.84	12.28
H_2O^-	0.08	0.28	0.14	0.36	0.06
Total	100.33	(100.00)	100.12	100.75	101.18

Atomic ratio on the basis of 14 oxygen atoms

Si^{4+}	2.730	4.000	2.687	4.000	2.844	4.000	3.096	4.000	9.852	4.000
Al^{3+}	1.270		1.313		1.156		.904		1.148	
Al^{3+}	1.155	6.019	1.236	6.030	1.071	6.033	.791	6.002	1.060	6.022
Fe^{3+}	.074		.019		.021		.113		.044	
Fe^{2+}	—		.238		.527		.553		.736	
Mn^{2+}	.054		.017		.024		.008		.007	
Mg^{2+}	4.736		4.520		4.390		4.537		4.175	
Ca^{2+}	—		—		—		—		—	

1. Chlorite (manganoan leuchtenbergite) in a metamorphosed manganese ore deposit at Muramatsu, Nagasaki Prefecture[16] (collected by Y. Okamoto).
2. Chlorite in the skarn of the Kamaishi mine, Iwate Prefecture (Kō Collection of Kyushu University). The analysis corrected for 0.2% calcite impurity.
3. Chlorite in serpentinite at Sannō, Fukuoka Prefecture (collected by H. Shirozu).
4. Chlorite forming a vein accompanying talc in serpentinite at Okushi, Nagasaki Prefecture (collected by K. Muta).
5. Chlorite forming a vein in serpentinite at Wakimisaki, Nagasaki Prefecture[17] (collected by T. Oshima, specimen T52).

Table 1.—*Continued*

No.	6	7	8	9	10	11
SiO_2	29.73	26.04	25.75	24.56	22.81	23.38
Al_2O_3	17.95	19.96	19.18	16.07	20.35	19.32
Fe_2O_3	0.68	1.85	2.51	5.10	4.84	2.51
FeO	10.05	21.34	28.21	34.66	34.87	38.38
MnO	8.24	0.47	0.82	1.42	0.56	0.58
MgO	21.84	18.56	12.77	6.16	6.11	5.39
CaO	none	—	none	0.30	0.10	tr.
H_2O^+	11.90	11.62	11.22	11.93	10.80	10.62
H_2O^-	0.42	0.16	0.43	0.54	0.23	0.48
Total	100.81	(100.00)	100.89	100.74	100.67	100.66

Atomic ratio on the basis of 14 oxygen atoms

Si^{4+}	2.976	4.000	2.694	4.000	2.740	4.000	2.797	4.000	2.537	4.000	2.633	4.000
Al^{3+}	1.024		1.306		1.260		1.203		1.463		1.367	
Al^{3+}	1.093		1.127		1.146		.953		1.204		1.196	
Fe^{3+}	.052		.144		.201		.436		.405		.212	
Fe^{2+}	.841	5.941	1.846	6.018	2.510	5.956	3.300	5.908	3.242	5.928	3.612	5.980
Mn^{2+}	.699		.041		.074		.137		.053		.056	
Mg^{2+}	3.256		2.860		2.025		1.045		1.012		.904	
Ca^{2+}	—		—		—		.037		.012		—	

6. Chlorite forming a veinlet in a manganese ore deposit of the Kumanohata mine, Shiga Prefecture (collected by T. Yoshimura).
7. Chlorite associated with a bedded cupriferous pyrite deposit (Yokeikosho) of the Besshi mine, Ehimé Prefecture (collected by M. Yamada). The analysis corrected for 0.9% calcite impurity.
8. Chlorite in a quartz-Cu ore vein (Shimo-4, Saisei-hi) of the Osaruzawa mine, Akita Prefecture (collected by K. Shinohara).
9. Chlorite associated with an iron containing silica stone deposit at Shōgasé, Kōchi Prefecture[21] (collected by H. Shirozu).
10. Chlorite in the quartz-Cu ore vein of the Sayama mine, Akita Prefecture (collected by K. Kinoshita).
11. Chlorite in a quartz-Cu ore vein (2-ban-ko, W-3-B) of the Kishu mine, Mié Prefecture (collected by the staffs of Kishu mine).

Table 2. X-ray powder data for 1-layer monoclinic chlorites

No.	1			4		7	
hkl	*d*(Å) calc.	*d*(Å) obs.	*I*	*d*(Å)	*I*	*d*(Å)	*I*
001	14.18	14.1	7	14.2	8	14.2	7
002	7.09	7.07	9	7.12	10	7.10	10
003	4.727	4.72	8	4.75	8	4.72	7
020	4.605	4.59	1				
004	3.545	3.54	10	3.56	10	3.54	10
005	2.836	2.84	5	2.85	4	2.83	4
131, 20$\bar{2}$	2.580	2.58	3	2.58	3	2.60	4
13$\bar{2}$, 201	2.538	2.53	6	2.55	5	2.56	4
132, 20$\bar{3}$	2.435	2.43	5	2.44	4	2.45	4
13$\bar{3}$, 202	2.378	2.37	4	2.38	2	2.39	3
133, 20$\bar{4}$	2.254	2.25	3	2.27	3	2.27	3
134, 20$\bar{5}$	2.063	2.06	1			2.07	½
007	2.026	2.026	2	2.04	2	2.02	1
13$\bar{5}$, 204	2.001	2.000	6	2.01	4	2.00	5
135, 20$\bar{6}$	1.880	1.883	3	1.891	2	1.888	2
13$\bar{6}$, 205	1.822	1.825	3	1.833	2	1.830	1
136, 20$\bar{7}$	1.712	1.73	½B	1.732	1		
13$\bar{7}$, 206	1.661	1.660	1	1.672	1	1.668	1
137, 20$\bar{8}$	1.564	1.562	4	1.577	3	1.570	4
060, 33$\bar{1}$	1.535	1.534	7	1.541	6	1.549	5
062, 331, 33$\bar{3}$	1.500	1.500	2	1.507	2	1.513	2
063, 332, 33$\bar{4}$	1.460	1.458	1				
0010	1.418	1.417	2	1.429	1	1.415	2
064, 333, 33$\bar{5}$	1.409	1.407	½				
13$\bar{9}$, 208	1.393	1.392	5	1.403	4	1.395	4
065, 334, 33$\bar{6}$	1.350	1.349	½				
400, 26$\bar{2}$	1.319	1.317	2	1.323	2	1.327	1
139, 20$\bar{1}\bar{0}$	1.319						
401, 26$\bar{3}$	1.299	1.297	½				
066, 335, 33$\bar{7}$	1.287	1.287	2	1.294	3	1.299	½
1310, 20$\bar{1}\bar{1}$	1.219	1.220	2	1.228	1	1.222	½
26$\bar{6}$, 404	1.189	1.190	½			1.196	¼
13$\bar{1}\bar{1}$, 2010	1.189						
0012	1.182	1.182	1	1.192	1	1.180	1

Table 3. X-ray powder data for 1-layer ortho-hexagonal chlorites

No.	10			11		9	
hkl	*d*(Å) calc.	*d*(Å) obs.	*I*	*d*(Å)	*I*	*d*(Å)	*I*
001	14.13	14.1	5	14.1	4	14.2	3
002	7.065	7.05	10	7.05	10	7.1	10
003	4.710	4.69	5	4.70	4	4.68	3B
020	4.675						
004	3.533	3.52	9	3.54	8	3.55	8
005	2.826	2.83	4	1.83	1	2.85	½
200	2.699	2.67	1	2.67	3	2.68	3
202	2.522	2.51	5	2.53	5≈	2.52	5≈
				2.47	1		
025	2.418	2.40	½	2.39	½	2.43	¼
204	2.147	2.14	4	2.15	1≈	2.15	2≈
007	2.019	2.02	2			2.03	¼
206	1.775	1.776	4	1.77	1B	1.77	1B
240	1.767						
060	1.558	1.559	5	1.558	6	1.557	5
062	1.522	1.523	3	1.521	4	1.521	3
063	1.479	1.479	4	1.479	1	1.480	½B
208	1.478						
064	1.426	1.424	1	1.423	1		
0010	1.413	1.412	3	1.416	1	1.422	1B
065	1.365	1.365	½				
400	1.350	1.347	½	1.345	1	1.343	½
401	1.343						
402	1.326	1.326	1	1.326	1	1.323	1
066	1.300	1.300	1	1.998	½	1.302	½
404	1.261			1.26	¼	1.26	¼
2010	1.252	1.253	1				
0012	1.178	1.179	2	1.180	½	1.183	½
406	1.171	1.171	½				

B: an unusually broad line. ≈ The head of a diffused band extending to the side of smaller spacings.

Table 4. X-ray powder data for a mixture of monoclinic and ortho-hexagonal chlorites

hkl		No. 8		
monoclinic	ortho-hexagonal	d(Å) calc.	d(Å) obs.	I
001	001	14.18	14.1	6
002	002	7.090	7.05	10
003	003	4.727	4.72	6
020	020	4.655		
004	004	3.545	3.53	9
005	005	2.836	2.83	4
	200	2.688	2.67	2
131, 20$\bar{2}$		2.606	2.60	1
13$\bar{2}$, 201		2.553	2.56	1
	202	2.513	2.51	2
132, 20$\bar{3}$		2.458	2.44	2
13$\bar{3}$, 202		2.399	2.39	2
133, 20$\bar{4}$		2.272	2.27	1
	204	2.142	2.14	1
134, 20$\bar{5}$		2.077	2.07	½
007	007	2.026	2.02	2
13$\bar{5}$, 204		2.013	2.00	3
135, 20$\bar{6}$		1.890	1.887	1
13$\bar{6}$, 205		1.831	1.829	½
	206	1.775	1.77	½
	240	1.759		
13$\bar{7}$, 206		1.668	1.668	1
137, 20$\bar{8}$		1.570	1.570	2
060, 33$\bar{1}$	060	1.552	1.553	4
062, 331, 33$\bar{3}$	062	1.516	1.517	2
	208	1.480	1.478	½
063, 332, 33$\bar{4}$	063	1.474		
0010	0010	1.418	1.418	3
13$\bar{9}$, 208		1.398	1.395	2
139 20$\bar{1}\bar{1}$		1.323	1.324	1
066, 335, 33$\bar{7}$		1.297	1.300	1
0012	0012	1.182	1.182	2

Indexing of powder patterns

The indexing of reflections and the calculations of spacings for two types were made in terms of the cells shown in Fig. 1, on referring to the results of structure studied by G.W Brindley and others[2] that b/a is exactly $\sqrt{3}$, and β of monoclinic cell corresponds exactly to the displacements of $a/3$ in the a-direction (three times of the monoclinic elementary cell regarded as ortho-hexagonal). For these terms, the formulae for monoclinic and ortho-hexagonal systems become following:

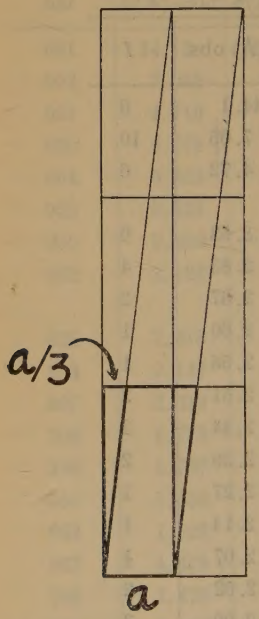

Fig. 1. Comparison of monoclinic and ortho-hexagonal elementary cells of chlorite. Projection of the cells on *ac*-plane is shown by heavy lines.

monoclinic ($a=b/\sqrt{3}$, $c\sin\beta=d_{001}$, $\cot\beta=a/3d_{001}$)

$$1/d^2=(3h^2+k^2)/b^2+(h+3l)^2/9d^2_{001}$$

ortho-hexagonal ($a=b/\sqrt{3}$, $c=d_{001}$)

$$1/d^2=(3h^2+k^2)/b^2+l^2/d^2_{001}$$

The results obtained from these formulae, being listed in Tables 2, 3, and 4, are satisfactory as a characterization of the powder patterns even though the exact cell shapes may be questionable.

1-layer (14Å) *monoclinic type*

This type is "normal chlorite type" by F. A. Bannister[10], and includes a large number of specimens which are chemically and also genetically different from one another, but Fe-rich members belonging to this type appear to be few so far in Japan. Although the variations in the intensities of the lines and/or the small changes in their positions caused by isomorphous substitution are observed, all the powder patterns are very similar, and the lines are generally moderately sharp. The data in Table 2 are those for nearly pure Mg-chlorite

(No. 1), Fe-containing Mg-chlorite (No. 4), and Fe•Mg-chlorite (No. 7), the specimen No. 4 contains relatively small amount of aluminum. Little differences are found among them.

1-layer (14Å) *ortho-hexagonal type*

Nearly all of the specimens belonging to this type are rich in iron and related to berthierine (kaolin-type chamosite), but at least a greater part of each specimen are clearly of chlorite-structure and are closely related to "chamosite" from Schmiedefeld, Thuringia[8] and also may be related to "daphnite" from Cornwall[6]. Fe-rich chlorites of this type are often found from various hydrothermal veins of metal mines, and this fact seems to be one of the characteristics of chlorites in Japan. Their powder patterns bear some resemblances to those of ortho-hexagonal berthierine[4], but give the characteristic basal reflections and the thermal behaviours of chlorite-type structure as already described on the minerals from Shōgasé* and Arakawa mine[21], and can be indexed in terms of a 1-layer ortho-hexagonal cell except a line (2.47Å) observed in specimen No. 11 (Table 3). However, the relative intensities, the sharpnesses, and/or profiles of lines of the Fe-chlorites belonging to this type are so variant to one another that they can be grouped from the general features into two: the minerals from Sayama (No. 10), Arakawa, etc., and those from Kishu (No. 11), Shōgasé (No. 9), etc. These points need further research.

Besides these Fe-rich members, a poorly crystalline Mg-rich chlorite closely associated with aluminian serpentine is considered as probably having an ortho-hexagonal cell, as will be presented in a separate paper of this Journal[22].

Mixture of monoclinic and ortho-hexagonal types

The above two types are often found from the same location, and

* The powder pattern and cell dimensions of the Shōgasé chlorite are reexamined and corrected in the present paper. The structural formula listed in Table 1 (No. 9) also seems to be more suitable than the previous one.

occasionally found as being closely associated with each other. The powder data shown in Table 4 are an example of the latter case, being interpreted as those of a mechanical mixture of the two types (under the microscope, this chlorite shows an intergrowth as mentioned later).

Cell dimensions

Determination of cell dimensions

The cell dimensions, d(001) and b, were determined for the chemically analyzed specimens from the (0010) and (060) reflection angles respectively by an X-ray diffractometer with filtered Co radiation as well as from the film-recorded data of high angles. Silicon powder was used as an internal standard. The results are shown in Table 5. The accuracy is about ± 0.01Å, in general, but d(001) for Nos. 9 and 11 includes errors of approximately ±0.03Å and ±0.02Å respectively because of their diffuse basal reflections.

Table 5. Cell dimensions of chlorites, and numbers of tetrahedral Al^{3+} and total Fe (including Mn) atoms in the ideal "orthochlorite" formula.

M: monoclinic. H: ortho-hexagonal

No.	1	2	3	4	5	6	7	8	9	10	11
Elementary cell	M	M	M	M	M	M	M	M+H	H	H	H
d(001)(Å)	14.18	14.17	14.21	14.30	14.20	14.24	14.16	14.18	14.21	14.13	14.15
b(Å)	9.21	9.22	9.23	9.24	9.24	9.28	9.29	9.31	9.34	9.35	9.35

No. of atoms assigning cations to the 4 tetrahedral and 6 octahedral positions

Al[4]	1.27	1.32	1.17	0.90	1.15	1.01	1.31	1.25	1.18	1.44	1.36
Fe(Mn)	0.13	0.27	0.57	0.67	0.79	1.60	2.03	2.60	3.91	3.73	3.89

Relations of cell dimension to chemical composition

The values of cell dimension obtained here indicate that the basal spacing decreases with the amount of tetrahedral $Al^{3+}(Al^{[4]})$, and the b value increases with Fe, as shown recently by many workers[8)1)5)14)11)7] (Table 5). In Figs. 2 and 3, the $d(001)$ and b values are plotted with solid circles against the numbers of $Al^{[4]}$ and total Fe (including Mn) respectively, which are calculated from the analyses assigning metal ions to the ideal chlorite formula presented before. Some previous data for chlorite and serpentine minerals are also plotted with open circles in these figures.

The curves for the present data show that the $d(001)$ and b of the two types have systematic relationship with the chemical composition. The values of basal spacing, $d(001)$, obtained here lie on a curve more satisfactorily than the previous values, some of them which are distant from the present curve may lie on or near the curve upon

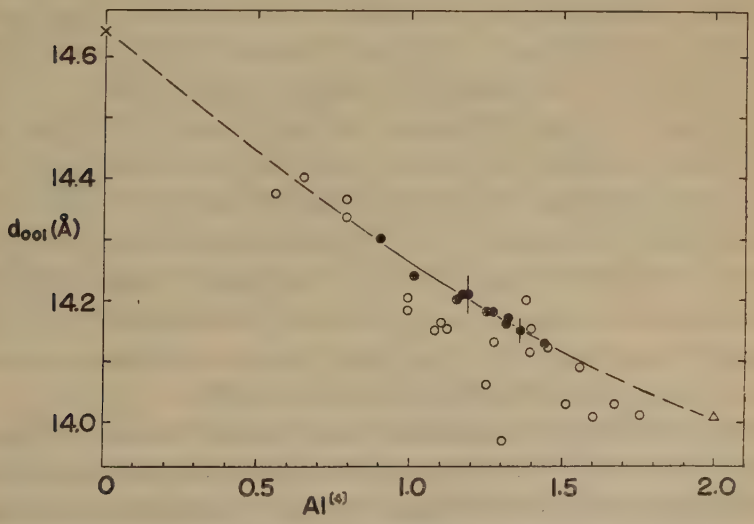

Fig. 2. Relation between basal spacing, $d(001)$, and tetrahedral Al content in chlorite. ● present data (cf. Table 5). ○ previous data[13)8)1)5)9)20)], × serpentine (chrysotile and lizardite)[23)], △ amesite[3)].

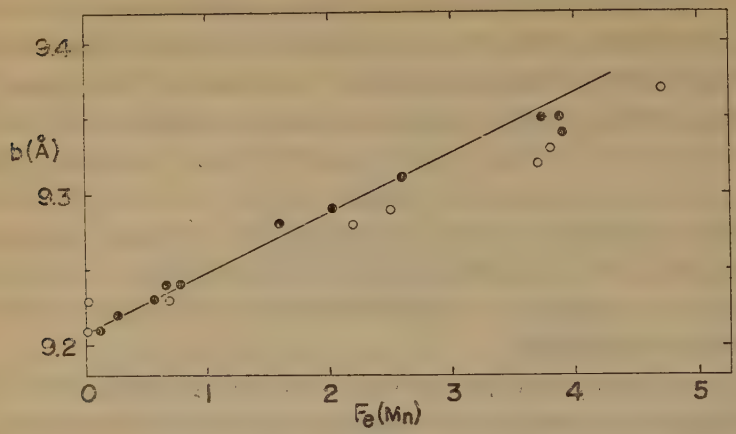

Fig. 3. Relation between b value and Fe (including Mn) content in chlorite. ● present data (cf. Table 5), ○ data given by Engelhardt[3].

more accurate determination of basal spacing by the use of high angle reflections (0010, 0012). A noteworthy fact on the basal spacings is that they are in harmony with those of serpentine and amesite on the amout of $Al^{[4]}$. The data for aluminian serpentines[15)18)19)] are also in harmony with this. Therefore, the basal spacings of chlorite and serpentine—aluminian serpentine—amesite series are considered that they have systematic relationship with the amount of $Al^{[4]}$ among the minerals with crystallinity of the same degree when we take the height of one chlorite layer and/or two serpentine layers. Although these polymorphic minerals are different in layer sequence, their basal spacings depend on the bonding forces between tetrahedral and octahedral layers, so this relationship may be natural.

The b dimension is considered to be effected by all the cations in the structure. In the chlorite structure, however, Al^{3+}(ionic radius, 0.57Å) substitutes both tetrahedral Si^{4+}(ionic radius, 0.39Å) and octahedral Mg^{2+}(ionic radius, 0.78Å) of about the equal amount, so that the effects by these ions are canceled mutually and may become very small for the b dimension. Therefore, actually the b dimension is

considered to be related closely to the number of Fe(Mn) atoms (mainly Fe^{2+} ion: ionic radius, 0.83Å) in the chlorite structure as shown in Fig. 3; most of the specimens studied except a few contain very small amounts of Fe^{3+} and Mn^{2+}ions. (ionic radius, 0.67Å and 0.91Å respectively).

X-ray determination of chemical composition

From the curves in Figs. 2 and 3, we can estimate the chemical composition of usual chlorite by the *X*-ray powder method, while it is considered that we must take care of the freshness of the sample when it shows a deep green color suggesting its high Fe-content, because the oxidation of Fe^{2+} to Fe^{3+} has influences on the cell dimensions*. Although G. W. Brindley and F. H. Gillery[7] stated that the Fe content could be more reliably determined from structure factor than from the b dimension, I consider that the b dimension is still effective for Fe estimation of usual chlorite on taking the above caution.

The cell dimensions of a number of chemically unanalyzed specimens were determined approximately with the results that most of them are within the range of the eleven specimens presented here: $d(001)=14.1\sim14.3$Å, $b=9.2\sim9.35$Å. This fact suggests that the Al-contents of the rather highly crystalline and commonly found chlorites are limited to a smaller range ($Al^{[4]}$ no.$=0.9\sim1.6$) than the previously considered, although the substitution of Fe to Mg takes a wide range, and as a whole, the chlorites with larger Fe-content appear to have a tendency to have larger Al-content.

A note on the interference colors

It is well known that chlorite frequently shows abnormal interference colors under the microscope, and their relations to chemical composition are made fairly clear by A. Hödl[12]. Most of the samples studied by him are probably of the monoclinic type; the here-examined

* An oxidized Fe-chlorite obtained with heating gave a little smaller b and larger $d(001)$ values than those before heating.

specimens giving the powder patterns of monoclinic type frequently show abnormal interference colors, in particular, agreeing with Hödl's conclusion, the chlorites containing rather large amount of Fe usually show the abnormal colors of ultra blue, reddish purple, reddish brown, etc. On the other hand, all of the Fe-chlorites belonging to the ortho-hexagonal type of powder pattern do show normal interference colors, and their retardations are rather high. Although this fact needs further optical study, it may be an important fact in distinguishing the two structural types by their microscopic characters.

Here is an interesting specimen, the Osaruzawa chlorite (No. 8), of which the powder pattern is a mixture of monoclinic and ortho-hexagonal types. Under the parallel nicols, flakes of this specimen have an appearance being homogeneous, but under the crossed nicols, these flakes consist of the alternations of thin lamellae with the abnormal interference color of reddish purple and those with the normal interference color of greyish yellow; namely, this specimen is an nearly parallel intergrowth of two polymorphic chlorites on *ab*-plane.

Acknowledgments

I with to acknowledge Professor T. Yoshimura of Kyushu University and Professor T. Sudo of Tokyo University of Education for their valuable suggestions and the gift of samples. Hearty thanks are also due to Professor K. Kinoshita, Professor T. Matsumoto, Assistant Professor S. Taneda, Lecturer Y. Okamoto, Mr. M. Yamaguchi, Mr. K. Muta, Mr. N. Tanaka, and Mr. M. Yoshinaga of Kyushu University, and to Professor K. Kinosaki of Hiroshima University, Mr. F. Hirowatari of Geological Survey of Japan, Mr. T. Oshima of Saga University, Mr. H. Yamamoto of Fukuoka Gakugei University, Mr. K. Shinohara of Mitsubishi Metal-mining Company, Mr. M. Miyahisa of Ehime University, Mr. M. Yamada of Zentsuji Daiich High School, and others, for the gift of valuable samples. Further, I wish to acknowledge a grant from the Government Expenditure for Scientific Research.

REFERENCES

1) Bannister, F.A. and W.F. Whittard: Min. Mag., **27**, 99 (1945).
2) Brindley, G.W., B.M. Oughton and K. Robinson: Acta Cryst., **4**, 552 (1951).
3) Brindley, G.W., B.M. Oughton and R.F. Youell: Acta Cryst., **3**, 408 (1950).
4) Brindley, G.W.: Mag., **29**, 502 (1951).
5) Brindley, G.W. and K. Robinson: Chap. VI of X-ray identification and crystal structure of clay minerals (1951).
6) Brindley, G.W. and F.H. Gillery: Proc. Second National Conference on clays and clay minerals, 349 (1954).
7) Brindley, G.W. and F.H. Gillery: Am. Min., **41**, 169 (1956).
8) Engelhardt, W. von: Zs. Krist., **104**, 142 (1942).
9) Frondel, C.: Am. Min., **40**, 1090 (1955).
10) Hallimond, A.F. and F.A. Bannister: Min. Mag., **25**, 441 (1939).
11) Hey, M.H.: Min. Mag., **30**, 277 (1954).
12) Hödl, A.: Neues Jahrb. Min., Beil-Bd., **77**, Abt. A, 1 (1941).
13) McMurchy, R.C.: Zs. Krist., **88**, 420 (1934).
14) Mikheev, V.I.: Zapiski Vsesoyuz. Min. Obschchestra, **82**, 214 (1953).
15) Nelson, B.W. and R. Roy: Proc. Second National Conference on clays and clay minerals, 335 (1954).
16) Okamoto, Y. and H. Shirozu: Mem. Fac. Sci., Kyushu Univ., D. **5**, 185 (1957).
17) Oshima, T.: Saga-daigaku Kyoiku-gakubu Kenkyu-ronbun-shu, **5**, 101 (in Japanese) (1955).
18) Roy, D.M. and R. Roy: Am. Min., **39**, 957 (1954).
19) Roy, D.M. and R. Roy: Am. Min., **40**, 147 (1955).
20) Sato, H. and T. Sudo: Min. Jour., **1**, 395 (1956).
21) Shirozu, H.: Min. Jour., **1**, 224 (1955).
22) Shirozu, H.: Min. Jour. (in press).
23) Whittaker, E.J.W. and J. Zussman: Min. Mag., **31**, 107 (1956).

Manuscript received Feb. 28, 1958

MINERALOGICAL JOURNAL VOL. NO. 4, PP. 224-235 JUNE, 1958

A STUDY ON MONAZITE FROM THE EBISU MINE, GIFU PREFECTURE

TOSHIO KATO

Mineralogical Institute, University of Tokyo

ABSTRACT

Monazite from the Ebisu mine, Gifu Prefecture has been studied. The monazite from Ebisu is of yellowish or dark brown colour, with sp. gr.: 5,20. The result of chemical analysis of the sample is as follows: P_2O_5 26.81, SiO_2 2,24, Al_2O_3 0.36, ThO_2 4.51, U_3O_8 0.21, Ce_2O_3 24.58, La_2O_3 etc, 38.51, Fe_2O_3 0.48, CaO 0.86, PbO 0.02$_6$, ig. loss 0.91, total 99.49% Monazites from Ratnapura, Ceylon and Minas Geraias, Brazil are also analysed for comparison. The relationships between the cell dimensions, the relative abundances of rare earths and the ThO_2 content are discussed. The chemical age of the Ebisu monazite is 108 m.y., while its thorium lead age on the basis of mass-spectrometric data is fifty million years, in accordance with the geological evidence.

Introduction

Neagi district, Gifu Prefecture, is one of the most famous localities of radioactive minerals in Japan. Recently the writer studied monazite from the Ebisu mine in the district, applying mass spectroscopic method and determined its absolute age.

The ages of several radioactive minerals from Japan have been determined by the chemical method, which is simply based on the ratio of total lead to uranium plus thorium in a mineral. This ratio will not give reliable age unless severe prerequisites are satisfied.

Occurrence

The Ebisu mine, Wada, Hirukawa village, Ena county, Gifu Prefecture, is situated about 14 kilometers north of the Oi railway station,

Chuo Line. The mine is worked for wolfram and arsenic. The geology of the district has already been reported by H. Shibata[9]. According to him, the geology of the district consists of quartz porphyry, granite porphyry, biotite granite and Palaeozoic formations. A granite mass, which contains numerous drusy pegmatites and has been specified as Naegi type by him, intruded and silicified the quartz porphyry. Its age is considered to be of late Cretaceous. The ore deposits of the Ebisu mine are composed of several pneumatolytic quartz veins accompanied by greisen in the quartz porphyry or in the granite. The ore minerals are wolframite, scheelite, molybdenite, bismuth minerals, arsenopyrite, etc. Monazite is found as small disseminated grains with the modes of occurrence of the following three types: the first, in quartz vein comprising wolframite and bismuth minerals; the second, in greisen containing topaz and micas; and the last, in the silicified country rock. It is of interest that a considerable quantity of monazite occurs in such modes as those and that similar cases have been revealed in several localities in Japan.

Physical properties

Monazite from the Ebisu mine seldom shows crystal faces. It is yellowish to dark brown in colour with white streak. The hardness is 5, and specific gravity, determined by the pycnometer method, is 5.20 at 18°C. The indices of refraction are α 1.790, β 1.791, and γ 1.840; and $(+)2V=10°$.

Chemical analysis

The monazite sample was prepared from the wolframite concentrate which was kindly offered by the Ebisu Mining Company through the courtesy of Prof. N. Katayama. About 50 kg. of the wolframite concentrate was sized into three fractions, that is 60–80, 80–110 and 110–170 mesh. From each of them, monazite was concentrated first with a magnetic separator. The monazite concentrate thus prepared was purified by hand picking under the binocular microscope. The purified

sample was analysed chemically.

Monazite from Ratunapura, Ceylon and from Minas Geraias, Brazil were also analysed for the sake of comparison.

Spectroscopic analyses revealed that the samples did not contain noticeable amount of element other than those chemically analysed.

The outline of the procedure of a quantitative analysis applied to the samples is as follows:

About 1 g. of the material was decomposed with about 10 ml. of boiling concentrated sulphuric acid for 30 min. After cooling, the decomposite was poured into 100 ml. of 2 per cent. sulphuric acid solu-

Table 1. Chemical analyses of monazites from Ebisu, Ratnapura and Minas Geraias

	1	1a	1b	2	2a	2b	3	3a	3b
P_2O_5	26.81%	3.640		26.84%	3.591		28.57%	3.739	
SiO_2	2.24	0.336	4.640	2.46	0.390	4.075	1.18	0.177	4.121
Al_2O_3	0.36	0.070		0.43	0.076		1.08	0.205	
ThO_2	4.51	0.165		14.52	0.532		5.37	0.186	
U_3O_8	0.21	0.008		0.32	0.010		tr.		
Ce_2O_3	24.58	1.452		22.95	1.330		28.43	1.609	
La_2O_3 etc.	38.51	2.149	3.962	30.56	1.369	3.981	32.49	1.894	4.017
Fe_2O_3	0.48	0.058		0.93	0.116		2.88	0.334	
CaO	0.86	0.130		0.82	0.123		0.02	0.003	
PbO	0.026	0.000		0.20	0.001		0.09	0.000	
Ig. loss	0.91			0.35			0.46		
Total	99.49%			100.37%			100.57%		

[Analysis by T. Kato (1957)]

1 Monazite from the Ebisu mine, Gifu Pref.
2 Monazite fyom Ratnapura, Ceylon.
3 Monazite from Minas Geraias, Brazil.

a and b are molecular ratios and molecular proportions, reepectively

Chemical formula:

1. $(Ce_{1.45}TR_{2.15}Th_{0.17}Fe^{3}_{0.06}Ca_{0.13})(P_{3.64}Si_{0.31}Al_{0.07})O_{16}$
2. $(Ce_{1.33}TR_{1.87}Th_{0.53}Fe^{3}_{0.12}Ca_{0.12})(P_{3.59}Si_{0.39}Al_{0.08})O_{16}$
3. $(Ce_{1.87}TR_{1.89}Th_{0.19}Fe^{3}_{0.33}Ca_{0.00})(P_{3.74}Si_{0.18}Al_{0.20})O_{16}$

TR = Total rare earths except cerium.

tion. The SiO_2 was determined from the residue. The volume of the filtrate was adjusted to 250 ml. The 25 ml. portion was used to determine phosphorus, the 50 ml. portion to titrate cerium by ammonium ferrous sulfate and potassium permanganate after oxidizing cerrous to ceric ion by ammonium persulfate, and the 100 ml. portion to separate rare earths and thorium by oxalic acid and ammonium hydroxide, and

Table 2. Chemical analyses of monazites and huttonite

	1	2	3	4	5	2
Ce_2O_3	21.08%	27.77%	22.03%	19.44%	31.90%	
La_2O_3 etc.	31.27	28.15	38.57	23.24	28.00	2.6%
Y_2O_3 etc.	3.53	3.01			0.46	
ThO_2	11.08	6.49	5.53	8.52	10.22	76.6
U_3O_8	0.42	—	0.44		(0.37)	nil.
SiO_2	2.98	2.64	3.07	10.81	0.90	19.7
Fe_2O_3	0.66	1.33	1.52	nd.	1.50	1.2
P_2O_5	27.52	29.10	26.41	20.42	26.82	trace
H_2O^+	0.56	0.64	1.38	1.64	0.46	nil.
CaO	0.52	0.47	0.00	nd.	0.20	nil.
Al_2O_3	0.80	0.75	0.00	nd.	0.17	nil.
MgO	0.37	0.08	0.00	nd.	—	nil.
PbO	—	—	—	nd.	—	—
Total	100.69%	100.43%	100.39%		101.00%	100.1%
Sp. Gr.		5.11	5.0495			7.1

1. Monazite from Ishikawa, Fukushima Prefecture. Analysis by U. Shibata and K. Kimura (1921).
2. Monazite from Kuchinokura, Nara Pref. Analysis by T. Higami (1944).
3. Monazite from Kotogé, Fukuoka Pref. Analysis by T. Iimori (1936).
4. Monazite sand from Naegi, Gifu Pref. Analysis by U. Shibata and K. Kimura (1921).
5. Monazite from Travancore, Ceylon. Analysis by Johnstone (1914).
6. Huttonite from South Westland, New Zealand. Analysis by Hutton (1951).[2]

on the rare earths filtrate, iron, aluminium, calcium and manganese were determined.

In Table 1 are listed the results of the analyses of the monazites and in Table 2, some previous data for comparison.

X-ray fluorometric analysis

Semi-quantitative X-ray flluorometric analysis was carried out on the rare earths oxides which had been chemically separated from the monazite samples. The results recalculated on the basis of the sum of the intensities of CeLα and NdLα to be equal to 69.1 are shown in Table 3[4].

In reference to abundance, the rare earths in the monazites listed in Table 3 may be devided into three groups; the most abundant group comprising Sc and Y, the lanthanons with even atomic number, and the lanthanons with odd number.

Table 3. X-ray fluorometric data of monazite

Atom. No.	X-ray line	1 India	2 Ceylon	3 Thai	4 Ebisu	5 Ishikawa
57	$LaL\alpha_1$	10	11	6	8	8
58	$CeL\alpha_1$	45	33	38	38	28
59	$PrL\alpha_1$	15	13	10	8	10
60	$NdL\alpha_1$	24	25	25	23	21
62	$SmL\alpha_1$	23	24	23	20	24
63	$EuL\alpha_1$	9	8	11	11	10
64	$GdL\alpha_1$	32	27	31	26	33
65	$TbL\alpha_1$	6	5	7	7	7
66	$DyL\alpha_1$	66	60	44	25	66
67	$HoL\alpha_1$	8	10	15	18	25
68	$ErL\alpha_1$	8	3	6	7	16
69	$TuL\alpha_2$	6	5	9	7	8
70	$YbL\alpha_1$	17	9	12	11	13
71	$LuL\alpha^1$	9	5	6	4	8

Norelco spectrographic equipment, Target Mo, 40 kV, 15 mA. Analysing crystal LiF, line intensities were determined by the automatic scanning-recording method.

It is generally accepted that a Z-even lanthanons is always more abundant than Z-odd lanthanons of adjacent atomic number, and present data are in accordance with general trends.

The relative intensities of the $L\alpha_1$ lines of the individual rare earth-elements in the five monazite samples have been plotted against the content of thoria in Fig. 1.

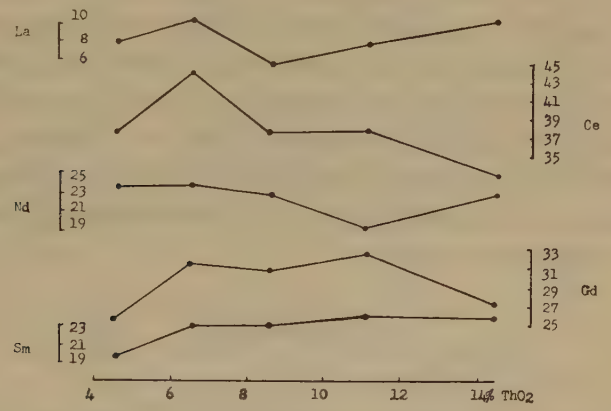

Fig. 1. Relative abundances of rare-earths in monazite.

Recently, Murata et al (1957)[4] analysed spectroscopically the rare earths in twenty-six monazite samples and showed that the contents of La and Ce increase together, and those of Nd, Sm, Gd and Y decrease concomitantly, while Pr remains nearly constant.

The data obtained by the present study do not necessarily follow their results as is obvious in Fig. 1.

X-ray examination

The X-ray powder patterns of monazites are compared in Tables 4-1 and 4-2 with that of huttonite.

Usually in monazite some thorium and a little uranium are present replacing cerium-lanthanum group elements. The increase in cation charge by the replacement is compensated for by the relevant replacement of phosphorus by silicon. The coupling replacement may

result in a solid solution series between monazite and huttonite, which have the same space group and the analogous crystal structure as monazite.

Although the cell dimensions of huttonite are very close to those of monazite, it is expected that there is systematic variation in them from monazite to huttonite.

On the other hand, Karkhanavara and Shankar (1944) and Ueda (1955)[13] proved by the X-ray powder method that some specimens of monazite were slightly metamict and lattice distension had taken place.

By using the spacings for powder lines which were calibrated by lead nitrate, the unit-cell dimensions of the raw specimen and the ignited specimen have been computed and the results are summarized in Table 5. The variation diagram of the cell dimensions versus ThO_2 content is illustrated in Fig. 2.

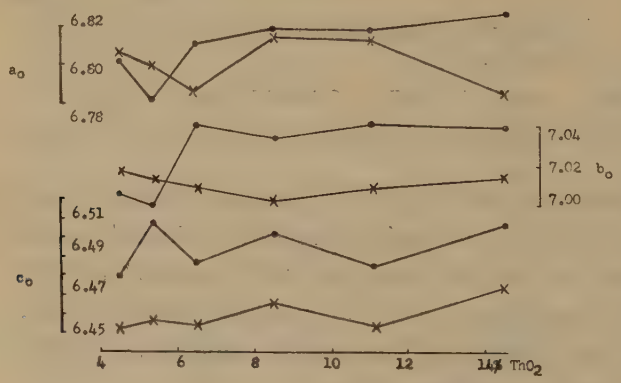

Fig. 2. Cell dimensions of monazite.

Contrary to the expectation, there is no systematic relationship between the cell dimensions and the thorium content of monazite. This may be attributable to the following facts. (1) The differences in cell dimensions between monazite and huttonite are too small to visualize the effect of the variation in thorium content. (2) In addition to the variation of thorium content, there is a complicated compositional variation in monazite.

Table 4-1. X-ray powder data of monazite and huttonite

hkl	1 monazite Ebisu			2 monazite Ishikawa			3 monazite Ceylon			4 monazite Brazil		
	d(Å)	*d*(Å)+	*I*	*d*(Å)	*d*(Å)+	*I*	*d*(Å)	*d*(Å)+	*I*	*d*(Å)	*d*(Å)+	*I*
$10\bar{1}$	5.25	5.20	10		5.19			5.23			5.23	
110	4.82	4.80	8	4.84	4.83	5		4.82		4.82	4.82	5
011	4.70	4.68	14	4.68	4.66	8	4.70	4.66	8	4.70	4.69	8
$11\bar{1}$	4.17	4.18	22	4.18	4.23	13	4.20	4.17	28	4.17	4.19	16
101		4.08		4.05	4.05	5	4.05			4.09	4.10	
111 020	3.51	3.51	30	3.50	3.51	25	3.52	3.51	36	3.51	3.52	16
200	3.30	3.30	60	3.34	3.31	20	3.30	3.30	50	3.34	3.30	20
120	3.09	3.09	100	3.09	3.09	100	3.10	3.09	100	3.10	3.10	100
210	2.98	2.986	22	2.996	2.988	10	2.996	2.987	20	2.994	2.987	12
012	2.877	2.827	45	2.877	2.864	80	2.877	2.864	53	2.873	2.866	80
$20\bar{2}$	2.611	2.624	11	2.609	2.628	8	2.611	2.59f	20	2.605	2.598	11
112	2.446	2.443	12	2.450	2.435	8	2.448	2.455	17	2.448	2.442	10
220	2.004	2.399	5	2.409	2.397	5	2.412		16		2.401	
931	2.198	2.191	30	29185	2.186	8	2.195	2.188	28	2.194	2.187	11
$10\bar{3}$ $31\bar{1}$	2.141	2.140	32	2.141	2.140	15	2.152	2.140	25	2.147	2.138	20
221		2.128		2.116	2.116	13	2.137		23	2.128		10
212	1.965	1.924	30	1.963	1.963	6	1.966	1.967	17	1.967	1.961	20
301		1.925		1.934	1.925	7				1.940	1.936	14
$23\bar{1}$	1.899	1.896	10	1.897	1.892	10	1.905	1.903	14		1.898	
103 032	1.877	1.866	15	1.875	1.877 1.870	10	1.870	1.373 1.869	28	1.875	1.874 1.868	20
320	1.876	1.860	15	1.861		5					1.861	
023		1.797			1.803		1.807	1.797	5	1.398		
222 040	1.768	1.765 1.753	10	1.762	1.758	12	1.759	1.755	5	1.763	1.756	6
132	1.743	1.737	16	1.745	1.738	11	1.743	1.739	10	1.742	1.742	14
321 140	1.692	1.689	10	1.693	1.688	8	1.688	1.693	17	1.694	1.694	4
123 400							1.663		5			

'Norelco' X-ray diffractometer. CuKα/Ni. 4-I-8 slit 1°, 0.006″, 1. Speed 1′/min. (partly 2′/min.) Scale factor 4′, Multiplier 1. Time constant 8 sec. *d*(Å) and *I* are the spacings and intensities for the raw specimen, respectively. *d*(Å)+ are the spacings for the ignited specimen.

Since the effect of ignition on the cell dimensions is very slight, the monazite from Ebisu may be considered to be almost free from metamictization.

The contents of uranium, thorium and lead in the monazite from the Ebisu mine, Gifu Presecture were determined chemically as follows;

Table 4-2. X-ray powder data of monazite and huttonite

(*hkl*)	1 monazite Thai			2 monazite India			3 nuttonite	
	d(Å)	*d*(Å)+	*I*	*d*(Å)	*d*(Å)+	*I*	*d*(Å)	*I*
$10\bar{1}$		5.17		5.22	5.28	12	5.29	3
100		4.81		4.80	4.76	17		
011	4.70	4.68	12	4.80	4.67	17	4.71	5
$11\bar{1}$	4.19	4.18	30	4.18	4.18	27	4.23	6
101		4.08			4.10		4.08	4
111	3.51	3.51	65	3.52	3.51	36	3.53	4
020							3.49	1
200	3.30	3.30	60	3.29	3.30	70	3.29	6
120	3.10	3.09	100	3.09	3.08	100	3.09	8
210		2.981	40		2.966	15	2.98	3
012	2.872	2.864	55	2.873	2.852	30	2.89	7
$20\bar{2}$	2.614	2.597	25	2.605	2.597	11	2.65	3
112	2.449	2.443	27	2.448	2.444	12	2.44	1
220	2.	2.399			2.393			
031	2.190	2.183	25	2.195	2.190	22	2.19	4
103	2.151		30	2.144		22		
$31\bar{1}$		2.137			2.144		2.156	2
221							2.110	3
212	1.970	1.967	30	1.973	1.967	12	1.953	4
301		1.945			1.949			
$23\bar{1}$		1.892			1.895		1.893	3
103		1.889			1.872			
032	1.863	1.866	35	1.868	1.663	22		
320							1.859	5
023		1.800			1.796			
222		1.767			1.768			
040	1.756	1.759	25	1.759		14	1.749	4
132	1.-47	1.742	25	1.743	1.741	17		
321								
140	1.694	1.691	20	1.694	1.677	12	1.692	4
123								
400							1.646	2

'Norelco' X-ray diffractometer. CuKα/Ni. 30 kV. 15 mA. 4 1-8 silt 1°, 0.006″, 1. Speed 1′/min. (partly 2′/min.) Scale factor 4′, Multiplier 1. Time constant 8 sec.

Thorium and uranium were determined by the gravimetric method. Hexamine was used to separate thorium from rare earths. Uranium was precipitated as uranyl-phophate. Lead was determined by the colorimetric method by use of dithizone.

Lead was isolated from the sample by extracting it into dithizone. In order to determine the isotopic composition of the lead, following two methods were taken: 1) The extracted lead was converted

Table 5. Cell dimensions of monazite

	1 Ebisu	2 Ishikawa	3 Ceylon	4 Brazil	5 Thai	6 India	7 Huttonite
raw specimen							
a_0	6.820Å	6.820	6.843	6.782	6.813	6.820	6.80
b_0	7.003Å	7.040	7.041	6.920	7.030	7.039	6.96
c_0	6.480Å	6.485	6.506	6.508	6.503	6.485	6.54
β	103°39′	103°47′	103°43′	103°45′	103°47′	104°00′	104.9°
Vol.	299.6Å	302.5	304.4	296.7	302.6	302.5	299
ThO_2	4.51%	11.25	14.52	5.37	8.50	6.54	76.6
after ignition							
a_0	6.806A	6.819	6.793	6.800	6.787	6.819	
b_0	7.016Å	7.006	7.015	7.013	7.002	7.005	
c_0	6.452Å	6.454	6.472	6.455	6.469	6.454	
β	103°34′	103°41′	103°44′	103°43′	103°46′	103°52′	
Vol.	295.1Å^3	298.9	298.9	299.0	298.0	299.6	

through lead iodide to tetramethyl lead by a reaction with Grignard solution[8]. 2) The extracted lead was converted through lead iodide to lead chloride. The products thus obtained were introduced in the mass spectrometer. The isotopic abundances were calculated after necessary corrections had been made. The obtained data are shown in Table 6.

The crude age read from graphs of Wickman's family[14] is 108 m. y. which is considerably higher than the probable age.

Table 6. Monazite from Ebisu

Th: 3.97%, U: 0.18%, Pb: 0.024%

Lead isotope	Pb^{204}	Pb^{206}	Pb^{207}	Pb^{208}
Isotopic constitution (moles)	1.9	48	41	100
Common lead″	1.4	25.7	20.8	51.5
Radiogenic lead (p.p.m.)	0	20	1	112
Age in 10^7 y.	U^{238}/Pb^{206} 8		Th/Pb^{208} 5	

″ Average ratio determined on the common lead by the writer.

The isotopic constitution of the lead in Table 6 is stated in proportions relative to Pb^{208} taken as 100.

From the geochemical point of view, it is expected that lead, apart from radiogenic lead, would be only of trace amount in monazite. Assuming that all of Pb^{204} is derived from common lead, the corresponding proportions of Pb^{206}, Pb^{207} and Pb^{208} were subtracted. Of the four isotopic ratio ages, the actinium lead age and the lead leod age are not reliable owing to the extremely small content of Pb^{207}. The remaining two ages, the thorium lead age and the uranium lead age, are rather similar, but, of the two ages, the thorium lead age is more accurate because the thorium contained in the monazite is of considerably large amount while the uranium is of very small amount.

Recently, Tilton et al. (1957)[10] reported the results of four isotopically controlled age determinations on monazites and of acid washing experiments and discussed the cause of the discordant age. However it was impossible to apply their procedure to the present data, because the age of the Ebisu monazite is too young.

Summary and discussion

The monazite from the Ebisu mine occurs in greisen and pneumatolytic quartz veins, and is chemically characterized in the thorium content which is lower than the usual monazite of pegmatitic origin. X-ray fluorometric analysis revealed that the relative abundance of rare earths is in accordance with the general tendency.

Since the effect of ignition on the cell dimension is very slight, the material used may be recognized to be almost free from metamictization. Besides, the material had been prepared from the wolframite concentrate which had been obtained from the ores mined at a stope far below the water level. Hence, it is suitable for the age determination.

The most reliable age obtained from the Th/Pb^{208} ratio, and revealed to be about fifty million years, corresponds to the earliest Tertiary or the latest Cretaceous age, which is acceptable from the geological point of view as well.

Acknowledgements

The writer wishes to express his sincere thanks to Prof. T. Ito, M.J.A. and Prof. N. Katayama for their valuable suggestions and guidances during the course of this work, and to Dr. R. Sadanaga and Dr. H. Minato for their critical discussions and advice. He also wishes to express his thanks to Prof. E. Minami, Dr. H. Sakai of the Chemical Institute, for their guidance in the work, and to Mr. H. Muraoka, Mr. Y. Iitaka and Mr. A. Kato for their aids. Thanks are also due to the officials of the Ebisu Mining Company, of the Nihon Denko K.K., and to Mr. Sato who kindly gave the specimen.

REFERENCES

1) Bowie, S.H.U. and Horne, J.E.T. (1953). Min. Mag. **30**, 93.
2) Hutton, C.O. (1950). Bull. Geol. Soc. Am. **61**. 636.
3) Murata, K.J. etal. (1953). Geochim. Cosmochim. Acta. **4**, 292.
4) ———, (1957). ibid. **11**, 141.
5) Pabst, A. (1951). Am. Min. **36**, 60.
6) ———. (1951). ibid. **36**, 557.
7) Sakai, H., Honda, M. and Minami, E. (1955). Bull. Chem. Soc. Jap. **28**, 535.
8) Sakai, H. (1956). Mass. Anal. No. 6, 37.
9) Shibata, H. (1939). Jour. Geol. Soc. Jap. **46**.
10) Tilton, C.R. and Nycolaysen, L.O. (1957). Geochim. Cosmochim. Acta. **11**, 28.
11) Ueda, T. (1953). Mem. Coll. Sci. Univ. Kyoto, B. **20**, 227.
12) ———. (1957). ibid. **24**, No. 2.
13) Ueda, T. and Korekawa, M. (1955). Min. Jour. **1**, 198.
14) Wickman, F.E. (1944). Arsbok Sveriges Geol. Undersok. **37**, No. 7.

Manuscript received March 20, 1958

Mineralogical Journal, Vol. 2, No. 4, pp. 236-244, June, 1958

MINERALOGICAL STUDY ON SOME PYROPHYLLITES IN JAPAN*

Hideomi Kodama

Geological and Mineralogical Institute,
Faculty of Science, Tokyo University of Education

Abstract

X-ray and chemical data of some specimens of pyrophyllite from Japan were discussed. The $k=3n$ reflections are predominant; this fact suggests that layers randomly displaced by multiples of $1/3b_0$ are dominant.

X-ray studies on ignited specimens have made clear a thermal transformation at 700°C, which agrees with the concept proposed by Bradley and Grim.

X-ray, thermal and chemical data on the 25 Å-clay mineral found in association with a certain specimen of pyrophyllite were discussed. The clay mineral agrees with a regularly interstratified pyrophyllite-montmorillonite.

Introduction

Many pyrophyllite deposits have been found, particularly in the central region of Japan, accompanying with kaolin minerals such as dickite and kaolinite, high aluminous minerals as diaspore and corundum. Most of these deposits have been worked as mineral resources of the fire-clay and paper industries and studied from the viewpoint of the economic geology, but their mineralogical studies are still scarce at present. This report will provide some mineralogical data of pyrophyllite found from the following three reference localites: (a) the Honami Mine, Nagano Prefecture; specimens (H-1), (H-2), (H-3), (H-4) and (H-5). (b) the Ônuki Mine, Tochigi Prefecture; specimen (O-1).

* Read at the symposium of the Japanese Group of Clay Research held in Tokyo on Nov. 1, 1957.

(c) the Yoji deposit, Gumma Prefecture; specimen (Y-1). All of these are hydrothermal replacement deposits in silicified andesite, liparite and shale respectively.

Specimens

The specimens used in this study are greasy, compact masses of fine crystal powders. The Honami materials show various colours as pale blue, pale green, bluish yellow, yellowish brown and grey. The other specimens show white or grey colours. Materials for studies were obtained by hand picking.

X-ray and chemical data

Chemical compositions and structural formulae of some reference

Table 1. Chemical compositions and structural formulae for some specimens of pyrophyllite from Japan.

	(H-1)	(H-2)	(H-3)	(H-4)	(H-5)*	(Y-1)
SiO_2	63.57%	64.02%	62.85%	63.79%	59.40%	62.02%
TiO_2	0.04	0.09	0.76	0.47	0.46	—
Al_2O_3	29.25	29.60	29.57	29.55	29.03	32.24
Fe_2O_3	0.10	0.16	0.11	0.20	0.34	tr.
FeO	0.12	0.08	0.10	0.14	0.34	tr.
MnO	none	none	none	none	0.01	none
MgO	0.37	0.45	0.25	0.33	1.98	0.18
CaO	0.38	0.12	0.08	0.07	0.90	0.40
K_2O	tr.	tr.	tr.	tr.	0.28	—
Na_2O	0.02	0.01	tr.	tr.	0.16	—
$H_2O(+)$	5.66	5.45	5.29	5.37	5.72	6.02
$H_2O(-)$	0.66	0.84	0.66	0.24	1.77	
P_2O	tr.	tr.	0.25	0.02	0.14	—
Total	100.17	100.82	99.92	100.18	100.53	100.86

* Specimen including mixed-layer mineral.

(H-1) Pale blue, $Ca_{0.02}(Mg_{0.03}Fe''_{0.01}Al_{1.97})(Al_{0.13}Si_{3.87})O_{10}(OH)_2$

(H-2) Pale green, $Ca_{0.01}(Mg_{0.04}Fe'''_{0.01}Al_{1.95})(Al_{0.14}Si_{3.86})O_{10}(OH)_2$

(H-3) Bluish yellow, $(Mg_{0.02}Fe'''_{0.01}Ti_{0.01}Al_{1.93})(Al_{0.16}Si_{3.84})O_{10}(OH)_2$

(H-4) Yellowish brown, $(Mg_{0.03}Fe''_{0.01}Fe'''_{0.01}Ti_{0.02}Al_{1.99})(Al_{0.13}Si_{3.87})O_{10}(OH)_2$

(Y-1) Grey, $Ca_{0.03}(Mg_{0.01}Al_{2.07})(Al_{0.23}Si_{3.77})O_{10}(OH)_2$

Table 2. X-ray powder data for typical specimens of pyrophyllite.

	H-1		Y-1	
Indices	d(Å)	I	d(Å)	I
002	9.21	vs	9.12	vs
004	4.58	s	4.55	s
020, 11$\bar{1}$ 110, 021	4.40	ms b	4.40	m b
11$\bar{2}$, 111	4.17	m b	4.15	ms b
113*			3.27	w
006	3.08	vs	3.07	vs
11$\bar{5}$, 114	2.97	vw		
130	2.59	w		
200, 13$\bar{2}$	2.55	mw	2.54	mw
20$\bar{2}$, 132	2.44	m	2.43	m
008	2.31	w	2.30	mw
134, 204	2.17	w	2.17	w
20$\bar{3}$	2.09	w	2.09	w
13$\bar{5}$	2.07	w	2.06	w
136	1.895	vw	1.899	w
0010	1.848	m	1.851	m
20$\bar{8}$	1.692	w	1.692	vw b
138	1.650	mw b	1.650	mw
0012	1.542	w		
060	1.492	mw	1.492	w
062, 33$\bar{2}$	1.475	vw		
1310	1.437	vw		
2010	1.388	mw	1.387	mw
13$\bar{1}$2	1.373	mw	1.369	mw

Intensities are: vs; very strong, s; strong, ms; moderate strong, m; moderate, mw; moderate weak, vw; very weak, b; broad lines.
* unreliable index.

specimens with various colours are shown in Table 1. Any remarkable variations were not noticeable in the chemical compositions of these specimens. Accordingly, it seems to be unreasonable that variations of colours are attributed to variations of the contents of major

chemical components.

Powder reflections of specimens (H-1) and (Y-1) were recorded by using X-ray diffractometer. Table 2 shows some X-ray powder data for these specimens. The other specimens were also studied by X-ray. On the basis of Gruner's data[2] of pyrophyllite (a_0=5-14 Å, b_0=8.90 Å, c_0=18.55 Å, β=99°55′, $a:b:c$=0.577 : 1 : 2.084), all of these reflections can be indexed. Comparing carefully the X-ray data of these reference specimens with one another, it is seen that the number of $k \neq 3n$ reflections is less and especially the (020), (111), (110) and (021) reflections which are superimposed on each other are diffuse more or less in all specimens. These experimental results seem to be attributed to the degree of random displacements of $1/3nb_0$, as well as particle sizes. Among the relative particle sizes estimated from the WARREN's approximate formula and also from Half-value breadths of the reflections, significant differences were not found. That they are in nearly same order (500–300 Å) will confirm that all these results depend on the random displacements.

Thermal changes

The reference specimen (H-1) was ignited at temperatures 300°C, 500°C, 700°C, 900°C and 1100°C. These ignited specimens were analysed by X-ray (Fig, 1). The (00l) Fourier syntheses were done on specimens in natural state, ignited at 300°C and 700°C. From the well-oriented aggregates, the reflected (00l) intensities were obtained by integrating the peak areas, and they were reduced to the structural factors on the assumption that the well-oriented aggregates could be regarded as an extended face of a single crystal having mosaic texture. The Fourier synthesis was obtained by these observed structural factors and the signs of the calculated structural factors (Table 3). In three electron density curves (Fig. 2) the major differences appeared in the electron density at the octahedral layer. According to Bradley and Grim's interpretation[1], the anhydride structure of pyrophyllite was formed by removal of hydroxyl water at 500°–700°C in heptaphyllite

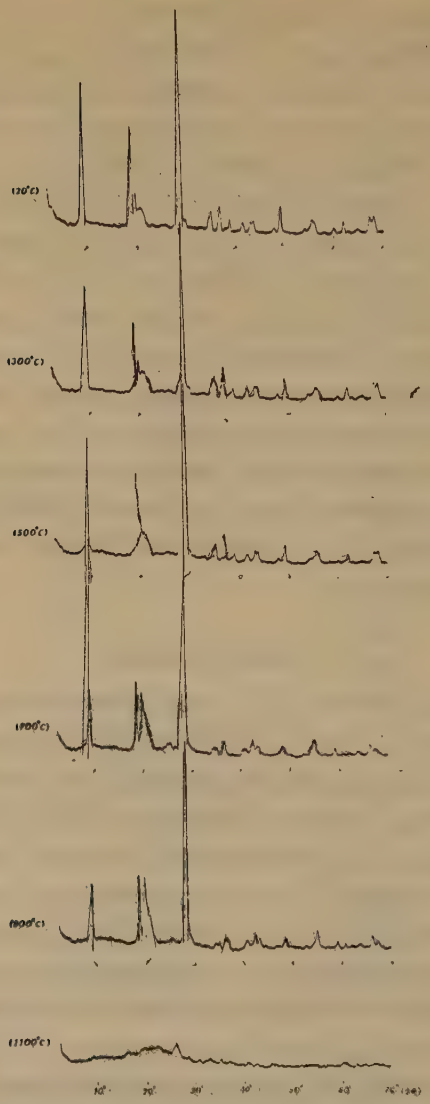

Fig. 1. Diffractograms of pyrophyllite in natural state and some pyrophyllites ignited at various temperatures.

type member and involved the expulsion of one-sixth of the oxygens of the octahedrally coordinated portion of the structure in the form of water. It seems that the Fourier synthesis of the specimen ignited at 700°C reproduced in Fig. 2 supports their concept. For the Fourier synthesis of the specimen ignited at 300°C, however, it is difficult to explain the cause of the decrease of the electron densities in anion sites at octahedral layer. The similar phenomenon was observed in illites treated at 350°C by Nelson[4]. The writer intends to advance more detailed analysis of the phenomenon, as it is possible that the removal of hydroxyl water may already start at about 300°C.

A regularly interstratified pyrophyllite-montmorillonite

The 25Å-clay mineral is found in association with pyrophyllite in specimen (H-5), which occurs in places along the marginal zone of the pyrophyllite deposit. X-ray powder reflections obtained from well-oriented aggregates consist of reflections of pyrophyllite and also the 25Å-clay mineral. As to the basal reflection of the 25Å-clay mineral,

Table 3. Calculated and relative structure factors for pyrophyllites.

F calc.		|F| obs.		
00*l*		Natural	300°C	700°C
002	+40	49	47	27
004	−54	57	51	40
006	+110	110	110	110
003	−30	33	19	—
0010	−70	58	37	23
0012	+32	36	20	18
0014	+68	47	23	18
0016	+58	46	—	—

only four basal reflections are available, because still higher order reflections overlap with those of pyrophyllite reflections (Fig. 3). The spacings of the basal reflections of lower order were obtained from the peaks recorded under a slow scanning speed. (Fig. 4. A)

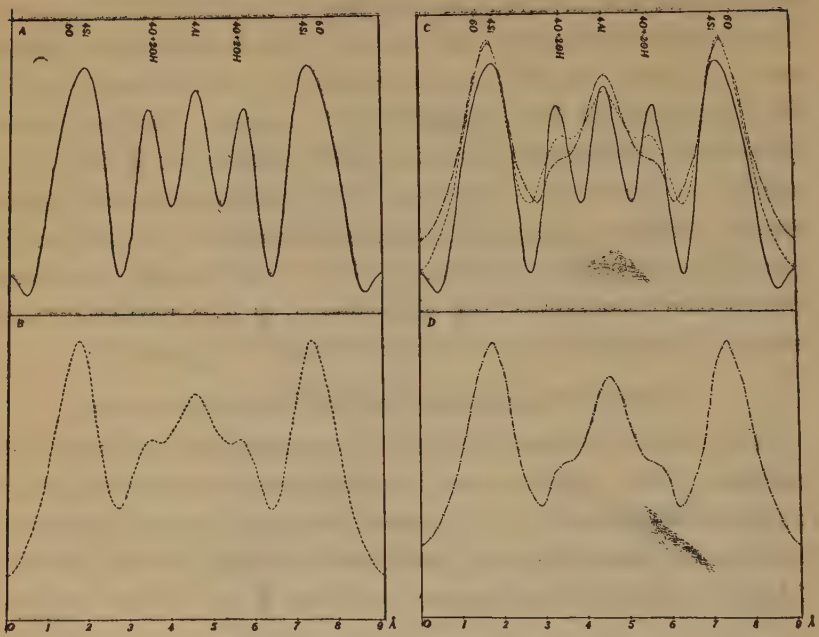

Fig. 2. Fourier synthesis curves.

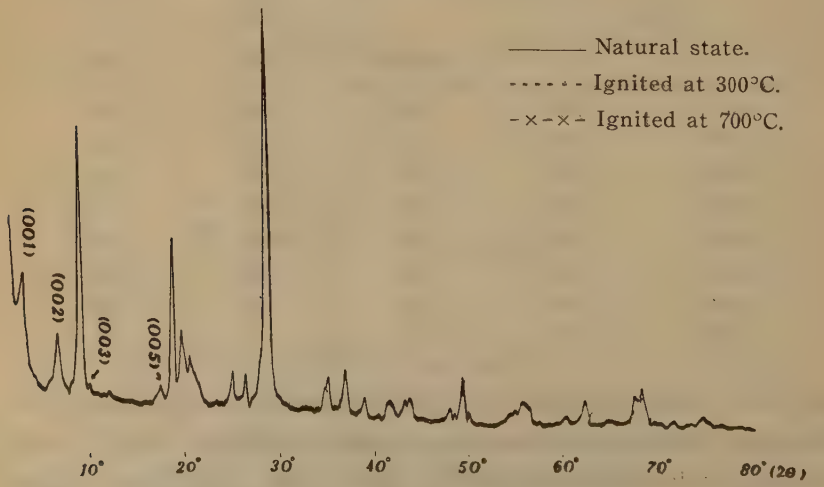

Fig. 3. Diffractogram of the 25Å-clay mineral found in association with pyrophyllite in specimen (H-5)

Treatment with ethylene glycol caused the 25.2Å reflection to be replaced by the 27.0Å reflection and the 12.5Å to 13Å (Fig. 4). The expansion of about 2Å suggests the presence of the montmorillonite lattice in this clay mineral. Fourier transform method after Mac-Ewan[3] was applied in this case. Transform from observed intensities for this 25Å-clay mineral is shown in Fig. 5. Well resolution between the 9.5Å (A peak) and 15.5Å (B peak) was obtained. Probabilities were obtained as follows:

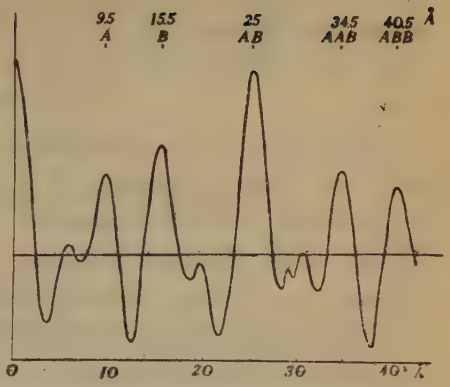

Fig. 5. Fourier transform from observed intensities for the 25Å-clay mineral.

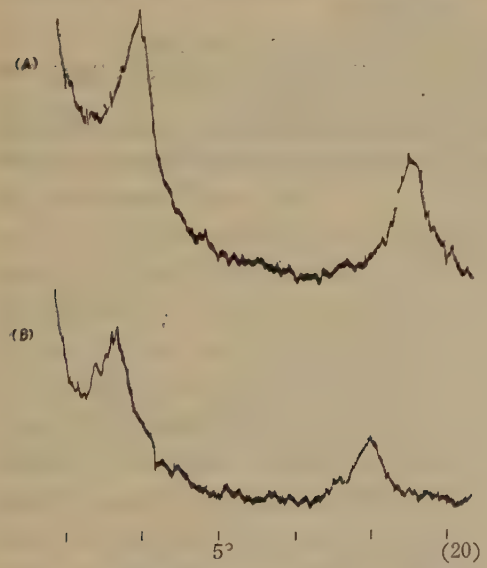

Fig. 4. Diffractograms of the basal reflections of the first and second orders recorded under a slow scanning speed.
A: in natural state,
B: treated with ethylene glycol

$P(AB)=0.96$, $P(AA)=P(BB)=0.04$, $P(A)=0.41$, $P(B)=0.57$.

These results indicated that the 25Å-clay mineral is largely composed of a regular alternation of 9.5Å and 15.5Å layers. The former is considered to be pyrophyllite and the latter to be montmorillonite. The bulk chemical composition of specimen (H-5) is shown in Table 1. Appreciable amounts of magnesium, calcium and water are considered to be

due to the presence of montmorillonite. In conclusion, the 25Å-clay mineral is a regularly interstratified pyrophyllite-montmorillonite.

Acknowledgements

The writer wishes to express his sincere thanks to Professor T. Sudô for his helpful suggestions and criticisms. Professor T. Sudô also carefully read this manuscript. Thanks are also due to Mr. M. Yoshida of the National Institute of Agricultural Sciences for his kind assistance in quantitative determination of alkalis.

The Honami Mine, the Ônuki Mine and the Joshin Chemical Mining Industrial Company supported the field work and provided the valuable specimens. On the occasions of indoor or field works, many persons encouraged him throughout the work, and their aid is gratefully acknowledged.

References

1) Bradley, W.F. and R.E. Grim.: Amer. Min., **36**, 183 (1951).
2) Bragg, W.L.: Atomic Structure of Minerals 212 (1937) Sec. Print. 1950.
3) MacEwan, D.M.C.: Koll. Zeit., **149**, 96-108 (1956).
4) Nelson, B.W,: Proc. Fourth National Conference on Clays and Clay Mineral. National Academy of Sciences-Nationatl Research Council. Publication **456**, 116-124 (1956).

Manuscript received in April 17, 1958.

Mineralogical Journal, Vol. 2, No. 4, pp. 245-268, June, 1958

INFRARED ABSORPTION AND STRUCTURES OF BORATE POLYATOMIC IONS

Yoshio Takéuchi

Mineralogical Institute, University of Tokyo

Abstract

The infrared absorption spectra of selected borate minerals have been observed with crystalline powders in the wavelength range from 2 to 16 microns. The spectra characteristic to borate polyatomic ions appear within the range from 7 to 16 microns and are presented in Figs. 1-6. These characteristic absorption bands are shown to be useful in the qualitative analysis of borate polyatomic ions.

In connection with this investigation, a discussion on the structures of borate polyatomic ions is also given.

Introduction

While examining the infrared absorption spectra of szaibelyite, $MgHBO_3$, for the purpose of investigating the state of hydrogen in the structure, fairy well defined absorption spectra were obtained in the wavelength range from 7 to 16 microns. It is obvious that these spectra in this range are due to the 'internal' vibrations of borate polyatomic ions in the structure of szaibelyite. A check shows that the absorption spectra are quite different from those previously reported of other borates such as boric acid or borax[11]. It appears therefore, that borate polyatomic ions possess frequencies which are sufficiently chracteristic to be useful for analytical purposes. Although extensive surveys of infrared absorption spectra of inorganic ions have been made[8)11)] and it has been proved that they are potentially useful for analytical use, the study on the borates of mineralogical importance has been neglected. It therefore seemed worth while to examine the infrared absorption spectra of thess borate minerals.

If the correlation between the infrared absorption spectra and the

structural types of borate polyatomic ions is made clear, it might well be possible to predict the structural types of polyatomic ions in borates whose crystal structures are unknown. This paper presents the spectra of 17 pure borate minerals and shows the relations between the spectra and structural types of borate polyatomic ions whose structures have so far been determined. Finally, the structures of borate polyatomic ions are discussed.

Experimental

Materials.

The samples used for the present investigation are listed below.

Sample	State of sample	Origin
kotoite	coarse powder	artificial
ludwigite	fibrous crystal	Suan Mine, Korea
pinakiolite	crystal	Långban, Sweden
suanite	fibrous crystal	Suan Mine, Korea
camsellite	matted fibrous	Douglas Lake, B.C.
sussexite	fibrous crystal	Sussex Co., N.J.
colemanite	crystal	Death Valley, Calif.
lesserite	crystal	Kern Co., Calif.
inderite	crystal	Kern Co., Calif.
meyerhofferite	crystal	Death Valley, Calif.
hilgardite	crystal	Iberville Parish, Louis.
ulexite	crystal	Ryan, Calif.
priceite	powder	Curry Co., Oregon
probertite	crystal	Kern Co., Calif.
kernite	crystal	Kern Co., Calif.
pinnoite	crystal	Stassfurt, Saxony
boron oxide	coarse powder	artificial

The samples obtained in well developed pure crystals were of highest purity. Other samples, especially, camsellite, priceite and pinnoite were carefully separated and examined under the microscope and by X-ray powder method and those of high purity were chosen for the infrared examination.

Spectroscopic procedures.

The samples were ground to fine powder to minimize the scat-

tering of light and rubbed between salt plates. All data were obtained on a Hilgar H 800 spectrometer, with a rock salt prism, using Nujol as the mounting medium. The region from 2 to 16 microns was scanned. No attempt was made to put the spectra on a quantitative basis which may not be necessary for the present purposes.

Results

The spectra in the wavelength range from 7 to 16 microns are shown in Figs. 1~6. The range well covers the characteristic absorption spectra of borate polyatomic ions. Some of the borate bands might exist in the regions of Nujol bands, however it does not limit the purpose of the present investigation. Fig. 8 sumarizes the positions of the spectra in wave numbers and gives roughly estimated peak intensities.

The absorption spectra of hydroxyl and water molecules are in the wavelength range from 2 to 7 microns. Although the interpretation of these spectra might give an interesting knowledge on the state of hydrogen atoms in the structures of hydrated borates, this is beyond the scope of the present work. However, some of them are shown in Fig. 7.

Absorption spectra of BO_3 groups.

BO_3 groups present most simple spectra and are well studied in the crystalline boric acid[7] and other simple orthoborates[14]. The absorption peak due to the fundamental modes such as totally symmetric stretch, ω_1 and out-of-plane bend, ω_2, are most characteristic for the group. The frequencies of these absorption peaks observed for kotoite, ludwigite and pinakiolite are as follows:

	$\omega_1(cm^{-1})$	$\omega_2(cm^{-1})$
kotoite	905	720
ludwigite	880	720
pinakiolite	850	720

The degenerate stretch, ω_3, gives very broad intense absorption peaks

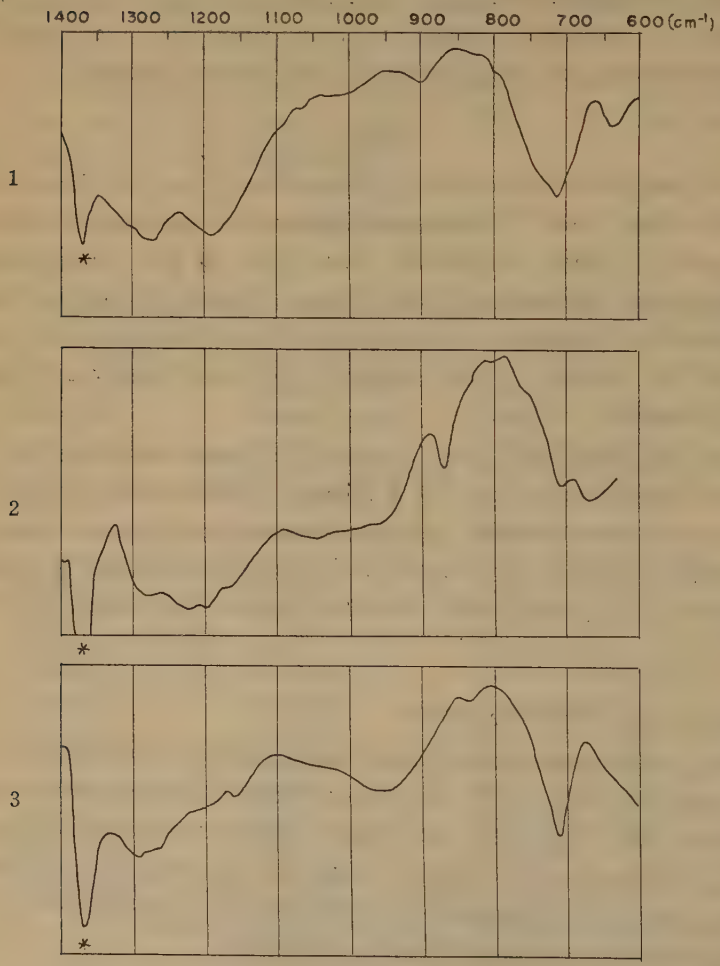

Fig. 1 Infrared absorption spectra of orthoborates.
1. kotoite, $Mg_2(BO_3)_2$
2. ludwigite, $2MgOFe^{3+}BO_3$
3. pinakiolite. $2MgOMn^{3+}BO_3$

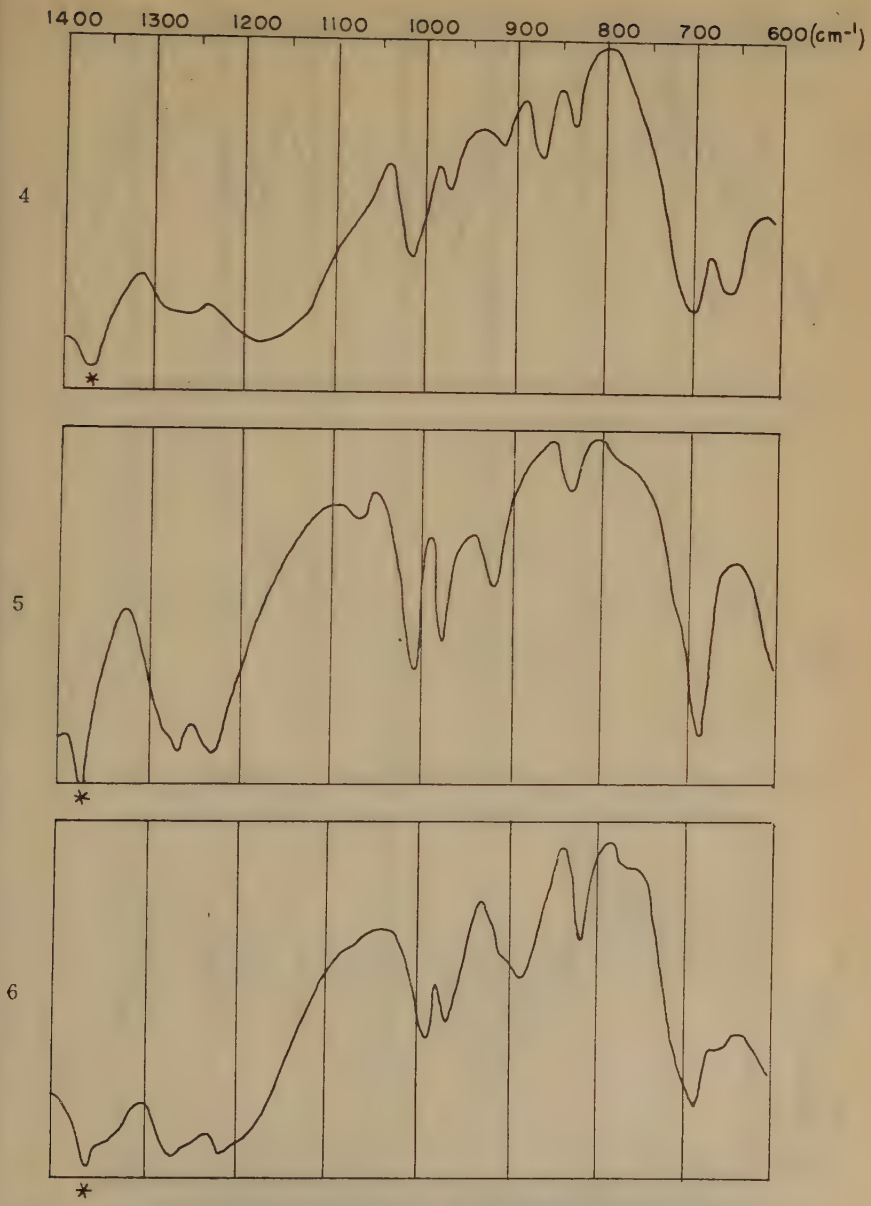

Fig. 2 Infrared absorption spectra of pyrborates with triangular configurations. 4. suanite, $Mg_2B_2O_5$ 5. camsellite, $MgHBO_3$ 6. sussexite, $MnHBO_3$

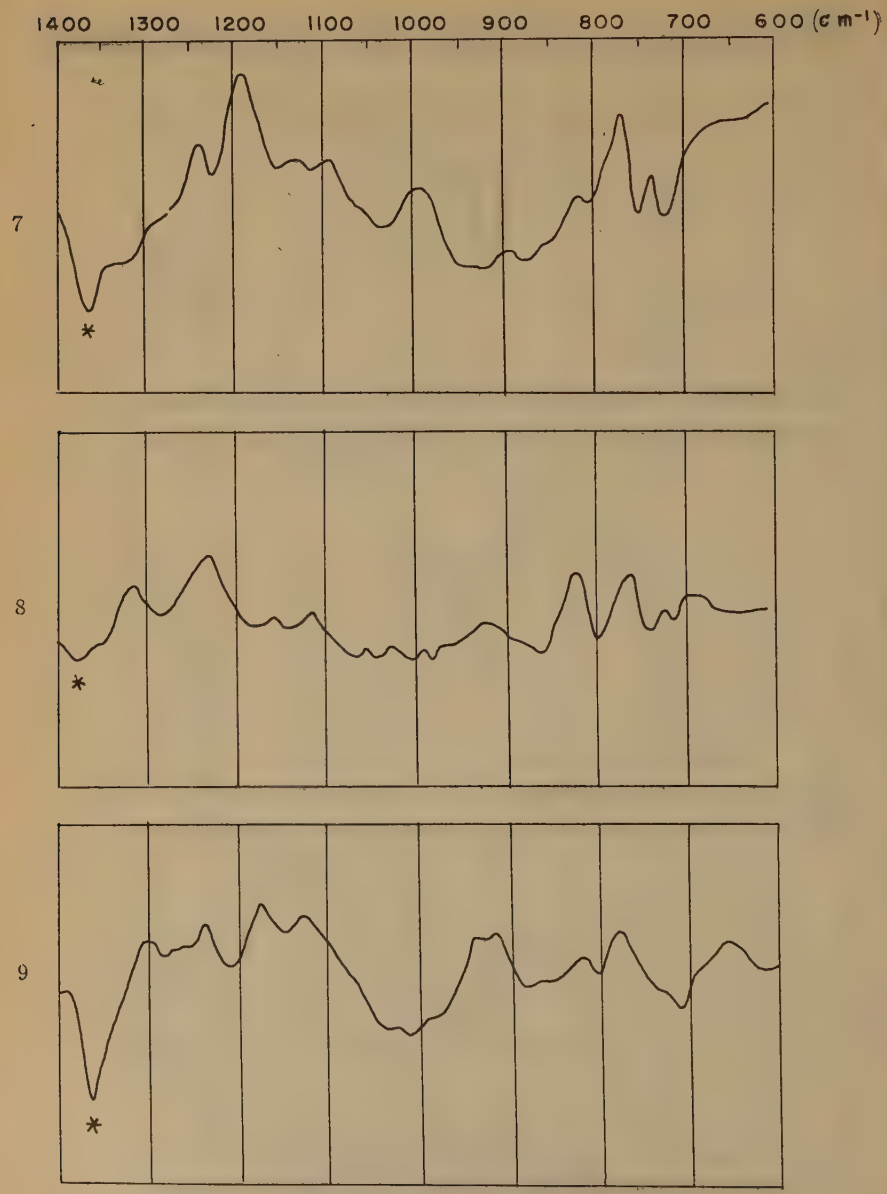

Fig. 3 Infrared absorption spectra cf borates.
7. colemanite, $CaH_3B_3O_7 \cdot H_2O$ 8. lesserite, $Mg_2B_6O_{11} \cdot 15H_2O$
9. inderite, $Mg_2B_6O_{11} \cdot 15H_2O$

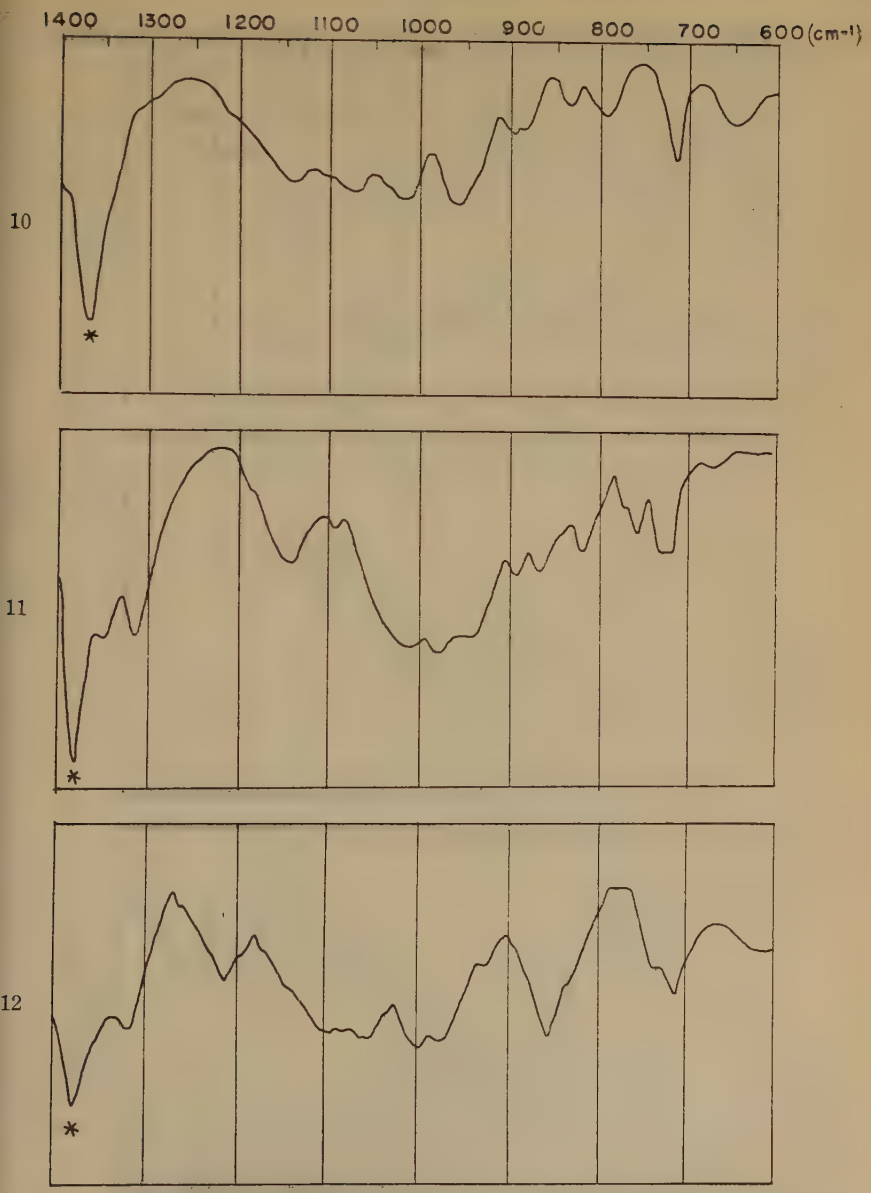

Fig. 4 Infrared absorption spectra of borates.
10. meyerhofferite, $CaH_5B_3O_8 \cdot H_2O$ 11. hilgardite, $Ca_3(B_6O_{11})_3Cl_4 \cdot 4H_2O$
12. ulexite, $NaCaB_5O_9 \cdot 8H_2O$

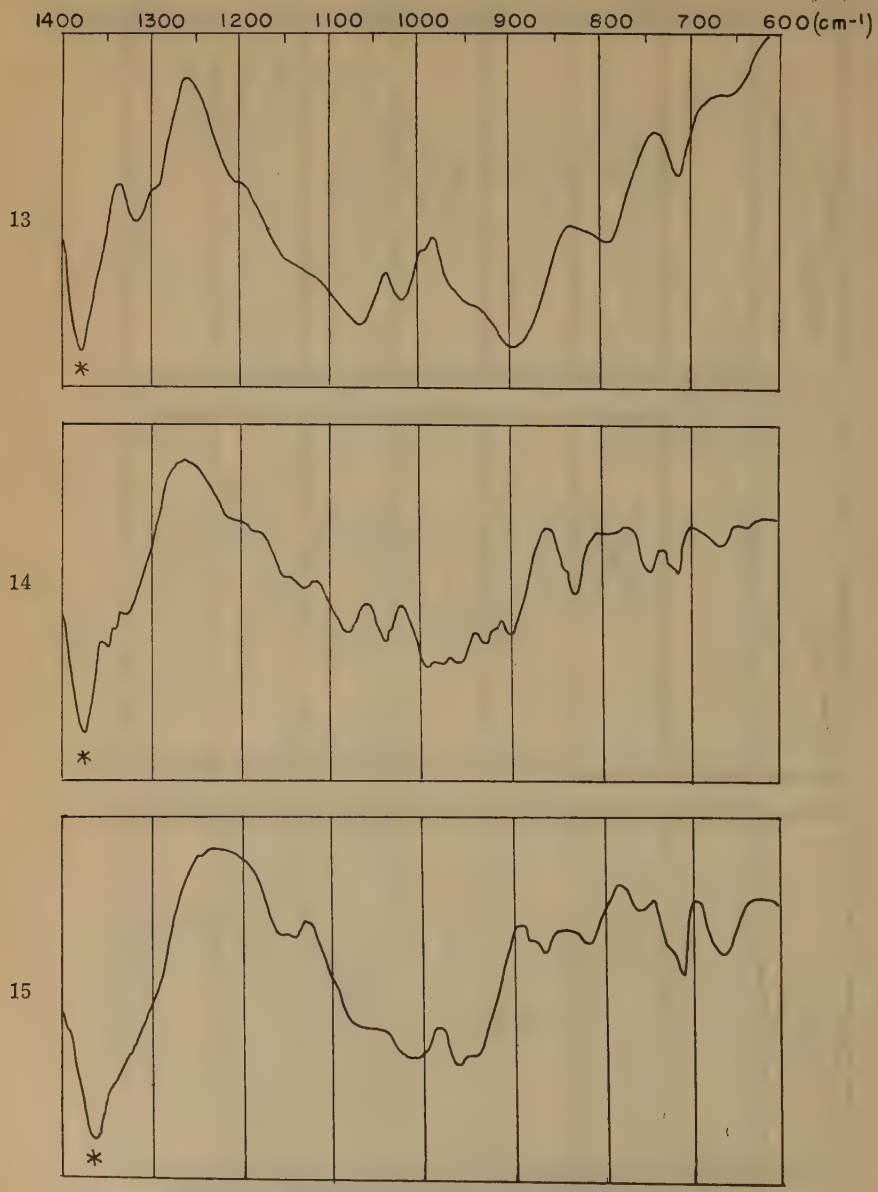

Fig. 5 Infrared absorption spectra of borates.
13. priceite, $Ca_4B_{10}O_{19}\cdot 7H_2O$ 14. probertite, $NaCaB_5O_9\cdot 5H_2O$
15. kernite, $Na_2B_4O_7\cdot 4H_2O$

around 1250 cm^{-1}.

It should be noted that totally symmetric stretch, ω_1, becomes inactive for some particular site symmetry of the BO_3 group[7]. The frequency difference as observed in these minerals may be due to the difference of the surrounding atoms of BO_3 groups in these structures[9)19)20)].

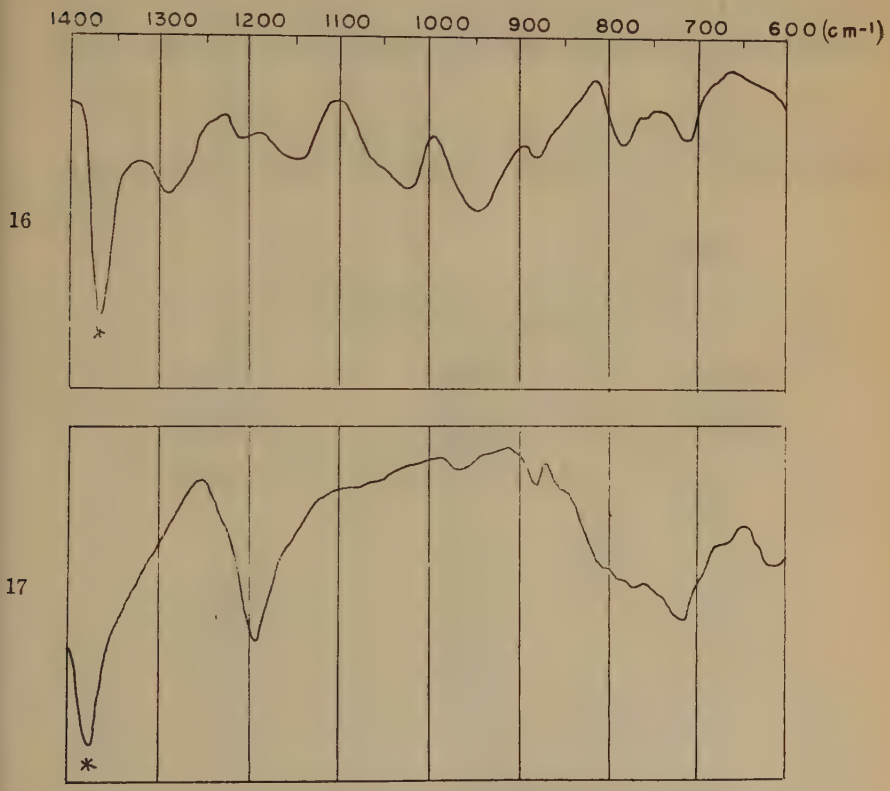

Fig. 6 Infrared absorption spectra of borate poylatomic ions with tetrahedral configurations.
16. pinnoite, $MgH_6B_2O_7$
17. boron oxide, B_2O_3
Nujol bands are marked with asterisks throughout Figs. 1-7.

Absorption spectra of B_2O_5 groups.

Suanite which contains (B_2O_5) groups presents well defined absorption peaks which are so characteristic that they are easily distinguished from those of the other borate polyatomic ions. It seems that the (B_2

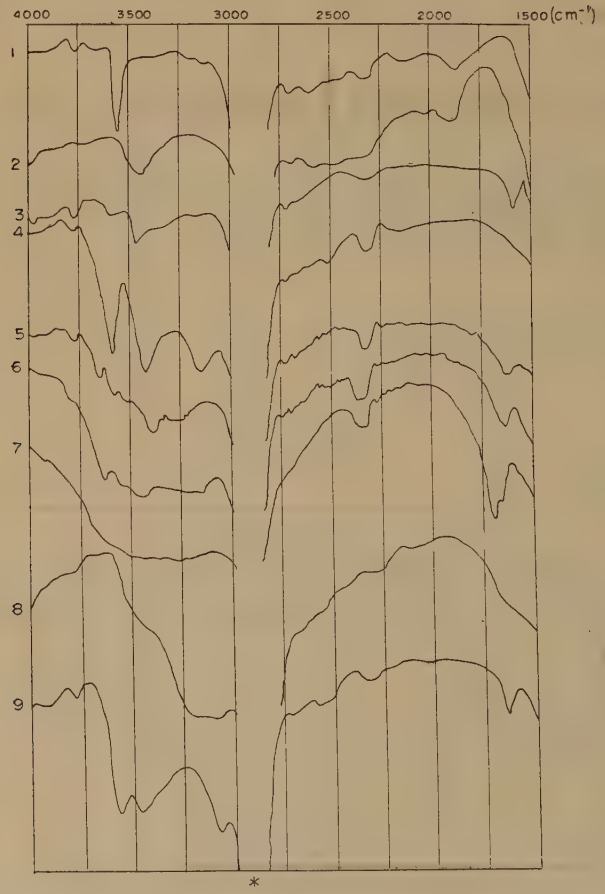

Fig. 7 Infrared absorption spectra of borates in the frequency range 4000–1500 cm^{-1}.

1. camsellite 2. sussexite 3. hilgardite
4. pinnoite 5. probertite 6. ulexite
7. lesserite 8. colemanite 9. priceite

O_5) groups exist not only in this rare mineral but also in camsellite (szaibelyite) and sussexite, because the absorption spectra of these minerals show striking similarity with those of suanite.

In this view point, the chemical formula of camsellite and sussexite may be expressed as $H_2Mg_2O(B_2O_5)$ and $H_2Mn_2O(B_2O_5)$ respectively. Thus, the unit cells of these borates contain four of these chemical units[16]. The extreme fibrous nature of these borates will be based upon a chain linkage of MgO_6 or MnO_6 octahedra as in magnesium orthoborates[17)19)] or in suanite[18)].

The frequencies of absorption spectra of suanite, camsellite and sussexite are compared in Table 1 together with estimated peak intensities.

Table 1. Infrared absorption spectra of pyroborates with triangular configurations.

suanite			camsellite			sussexite			
$Mg_2B_2O_5$			$MgHBO_3$			$MnHBO_3$			
I	Frequency (cm^{-1})		*I*	Frequency (cm^{-1})		*I*	Frequency (cm^{-1})		
			m	3552		m	3460		
			w	1900		w	1900		
s	1275	b	s	1270		s	1270	b	
s	1180	b	s	1230		s	1210	b	
w	1075	sh	w	1075					
m	1019		m	1010		m	992		
w	976		m	979		m	970		(B_2O_5)
w	921		m	921		m	910	b	spectra
m	872		vw	880	sh		885		
m	839		w	830		m	828		
			vw	775		vw	770		
s	705		s	690		s	695		
s	665					s	660		

sh = shoulder b = broad.

Absorption spectra of other borate polyatomic ions with triangular configurations.

In addition to the above groups, (B_2O_4) chain and (B_3O_6) ring structures are also known as with triangular configurations[21)25)]. The absorption spectra of the latter have been reported by F. A. Miller and C. H. Wilkins[11)], strong peaks of frequency 925 cm^{-1}, 1310 cm^{-1} and medium 1175 cm^{-1}, weak 862 cm^{-1} peaks being characteristic to the group. The spectra of (B_2O_4) chain structure were not obtained because of the difficulty of preparing crystals which contain this boron-oxygen linkage.

Table 2. Infrared absorption spectra of pinnoite.

I	Frequency (cm^{-1})	
s	3610	(OH)
s	3440	
s	3175	
s	1290	(B_2O_7)
w	1220	
m	1150	
m	1070	
s	1030	
s	960	
m	895	
w	800	
w	760	
w	720	

Absorption spectra of borate polyatomic ions with tetrahedral configurations.

Pinnoite $Mg(BO_2)_2 \cdot 3H_2O$ has (B_2O_7) polyatomic ions which consist of two BO_4 tetrahedra having one oxygen in common[13)]. The infrared absorption spectra of pinnoite are shown in Fig. 6. Frequencies of the observed peaks are given in Table 2.

The borates which contain separate BO_4 tetrahedra are rare. Teepleite, $Na_2H_4(BO_4)Cl$, would perhaps be the only one suitable to obtain the infrared data of BO_4 tetrahedron.

Absorption spectra of borate polyatomic ions with hybrid configurations.

The *hybrid configuration* which consists of a BO_3 triangle and a BO_4 tetrahedron (Fig. 9) is the most interesting subject in the studies of borate polyatomic ions. (B_4O_9) and (B_3O_8) groups and (B_3O_7) chain structures found in borax[12)], meyerhofferite[4)] and colemanite[3] respective-

ly are built of these cofigurations. The infrared spectra of these minerals are shown in Figs. 3 and 4.

Although the infrared peaks of these complicated borate polyatomic ions are not so well defined as those of simpler borate groups, they are still characteristic enough for analytical use. For instance, potassium tetraborate, $K_2B_4O_7 \cdot 5H_2O$, presents very similar spectra with those of borax[11]. It therefore seems probable that the crystal will contain (B_4O_9) groups rather than '(B_4O_7) ions' which has often been conceived by chemists. Thus the chemical formula of the substance may be written as $K_2H_4B_4O_9 \cdot 3H_2O$.

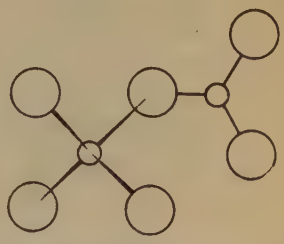

Fig. 9 Hybrid configuration of boron-oxygen arrangement.

As shown in Fig. 8 in the form of a line graph, the similarity of the spectra also suggests that inderite, $Mg_2B_6O_{11} \cdot 15H_2O$, is probably built up with (B_3O_8) polyatomic ions as meyerhofferite. For lesserite, the monoclinic polymorph of inderite[6], its spectra are analogous, in some ways, to those of colemanite but also similar to those of meyerhofferite. Therefore, no definite conclusion can be drawn for this case.

Borate polyatomic ions

Inspite of the formal analogy that (B_3O_6) rings and (B_2O_4) chains contained in most of metaborates correspond to (Si_3O_9) rings and (SiO_3) chains in metasilicates, the following two points may be mentioned as the characteristic differences between boron-oxygen arrangements and silicon-oxygen arrangements; Firstly, boron atoms may have either triangular or tetrahedral coordination and secondly, the bonds between boron and oxygen are less ionic than those between silicon and oxygen.

The partial ionic character for B–O and Si–O bonds may be estimated from the differences of electron negativity of these atoms. They are found as follows:

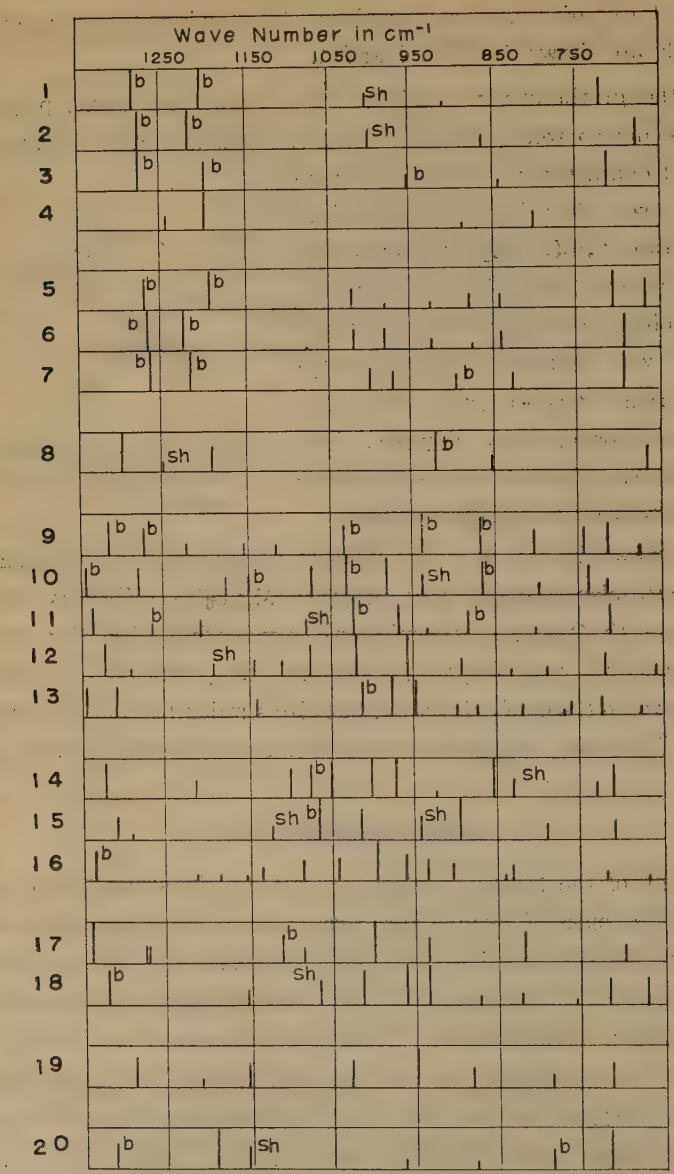

Fig. 8 Comparison of infrared spectra of borates. Positions of absorption spectra and estimated intensities are given.

Table for the explanation of Fig. 8.

	Substance	empirical formula	structural formula
1.	kotoite	$Mg_3B_2O_6$	$Mg_3(BO_3)_2$
2.	ludwigite	$2MgOFe_2O_3B_2O_3$	$2MgOFe^{3+}BO_3$
3.	pinakiolite	$2MgOMn_2O_3B_2O_3$	$2MgOMn^{3+}BO_3$
4.	*boric acid	H_3BO_3	H_3BO_3
5.	suanite	$2MgOB_2O_3$	$Mg_2B_2O_5$
6.	camsellite	$MgHBO_3$	
7.	sussexite	$MnHBO_3$	
8.	*sodium metaborate	$NaBO_2$	$Na_3B_3O_6$
9.	colemanite	$Ca_3B_6O_{11}5H_2O$	$CaH_3B_3O_7 \cdot H_2O$
10.	lesserite	$Mg_2B_6O_{11} \cdot 15H_2O$	
11.	inderite	$Mg_2B_6O_{11} \cdot 15H_2O$	
12.	meyerhofferite	$Ca_2B_6O_{11} \cdot 7H_2O$	$CaH_5B_3O_8 \cdot H_2O$
13.	hilgardite	$Ca_3(B_6O_{11})_3Cl_4 \cdot 4H_2O$	
14.	ulexite	$NaCaB_5O_9 \cdot 8H_2O$	
15.	priceite	$Ca_4B_{10}O_{19} \cdot 7H_2O$	
16.	probertite	$NaCaB_5O_9 \cdot 5H_2O$	
17.	*borax	$Na_2B_4O_7 \cdot 10H_2O$	$Na_2H_4B_4O_9 \cdot 8H_2O$
18.	kernite	$Na_2B_4O_7 \cdot 4H_2O$	
19.	pinnoite	$Mg(BO_2)_2 \cdot 3H_2O$	$MgH_6B_2O_7$
20.	boron oxide	B_2O_3	B_2O_3

* After F.A. Miller and C.H. Wilkins.[11]

b = broad Sh = Shoulder

Bond	Difference of electron negativity	Amount of ionic character
B-O	1.5	43%
Si-O	1.7	53%

The value of ionic character found for B-O bonds is indeed close to that of H-O bonds, the ionic character of H-O bonds being estimated as 39%, and B-O-B angles in borate groups will have more significant meaning than Si-O-Si bond angles.

Table 3. Bond angle for oxygen in borate groups.

Fundamental linkage of borate groug	Polyatomic ion	B-O-B angle
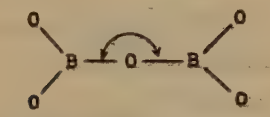	(B_2O_5) group (in suanite)	131.5°
	(B_5O_{10}) group	127°
	(B_3O_6) group	126.5°
	(B_2O_4) chain	130°13′
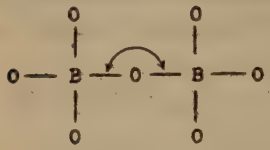	(B_2O_7) group	104°
	(B_4O_9) group	109°
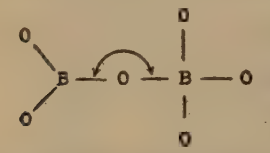	(B_4O_9) group	119°20′
	(B_5O_{10}) group	121°

Actually, the angles found by X-ray analysis in various borate polyatomic ions appear to have constant values for each fundamental linkage of borate groups (Table 3). Namely, for oxygen atom between two triangles, the angles are close* to the theoretical O⩽ angle, 125°16′. These observed bond angles are, however, larger than the theoretical one by about 4 %. This may be due to in the main the steric effects of BO_3 groups. For the case where the oxygen atom connects two BO_4 tetrahedra, the angles are very close to 109°28′ which is ex-

* The B-O-B bond angle of 153° found in $Co_2B_2O_5$ is exceptional.[2]

pected for O< bond angle. The angle for the oxygen atom of (B_2O_7) group found in pinnoite is markedly small. However, the value is less accurate because the structure of pinnoite was determined on the basis of the pseudo space group, $P4_2/n$, inspite of the evidence that the true space group of the mineral is $P4_2/m$. The real value of the bond angle might be closer to the tetrahedral bond angle. Although the final atomic parameters of colemanite and meyerhofferite have not been appeared, the similar bond angles are expected in the (B_2O_7) structural units in both the (B_3O_8) group of meyerhofferite and the (B_3O_7) chain of colemanite.

It is interesting to note that in the hybrid configuration where the oxygen atom is shared by a BO_3 triangle and a BO_4 tetrahedron, the bond angle for the oxygen atom takes the value in between of the other two cases discussed above.

It thus appears that the bonds between boron and oxygen are so strong and rigid that the oxygen bond angles found for the (B_2O_5) group in suanite and the (B_2O_7) group in pinnoite are always maintained in more complicated borate polyatomic ions which contain these groups as part of their polyatomic ions whatever the rest of the structures may be like.

These fundamental boron-oxygen groups are shown in Fig. 10.

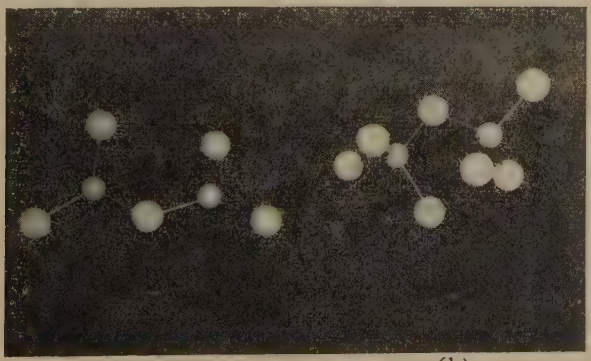

(a) (b)

Fig. 10 Fundamental configurations of boron-oxogen arrangements.
(a) B_2O_5 group as found in suanite.
(b) B_2O_7 group as found in pinnoite.

Other forms of separate boron-oxygen groups which have so far been found are shown in Fig. 11 where the (B_2O_5) and (B_2O_7) groups are indicated by thick lines for each group. Shapes of these two groups are also well preserved in boron-oxygen chains such as (B_2O_4) and (B_3O_7) which are shown in Fig. 12.

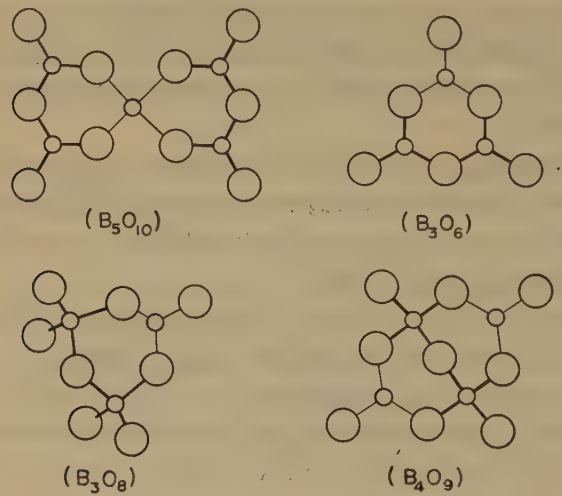

Fig. 11 Forms of separate boron-oxygen groups.
B_2O_5 and B_2O_7 groups are indicated by thick lines.

In many borate polyatomic ions, oxygen may be replaced to a certain extent by hydroxyl. The description of boron-oxygen arrangements through out this paper must therefore be taken to cover cases where partial replacement of oxygen by hydroxyl occurs.

Coordination of the boron atom.

Boron has been found at the center of either a tetrahedral group of four oxygen atoms or three oxygen atoms at corners of an equilateral triangle. The bond distances which have been found in three fold groups vary from 1.32 to 1.40 Å, and those in tetrahedral groups are around 1.47 Å (1.41 Å as found for BO_4 group in teepleite[5] and 1.56 Å in (B_2O_7) group of pinnoite[13] are the two extremes).

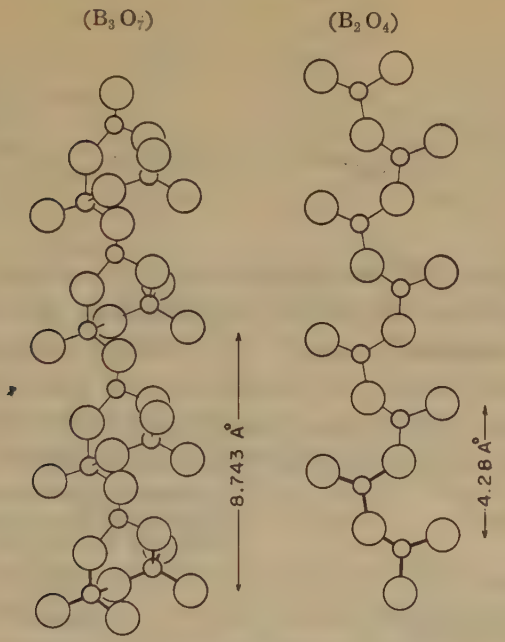

Fig. 12 Forms of boron-oxygen chains. B_2O_5 and B_2O_7 groups are indicated by thick lines.

As the shapes of these two groups are always regular, we must assume an intermediate state of the B–O bonding for the coordination of boron in boron oxide[1]. The B–O configuration in the boron-oxygen network of the crystal is observed to be of non-coplanar triangle with the B–O distances 1.48, 1.48 and 1.37 Å, the boron beeing placed 0.44 Å apart from the plane of this triangle. The boron atom is coordinated by another oxygen atom with the distance of 2.14_5 Å and thus the coordination of the atom has been described as a highly distorted tetrahedron of four oxygen atoms.

A similar acute oxygen pyramid with a boron inside and near the basal plane has been found in the boron-oxygen network of boracite[10] in which the distance between boron and oxygen at the apex of the pyramid is calculated as 1.78 Å. This kind of boron coordination is shown in Fig. 13 c.

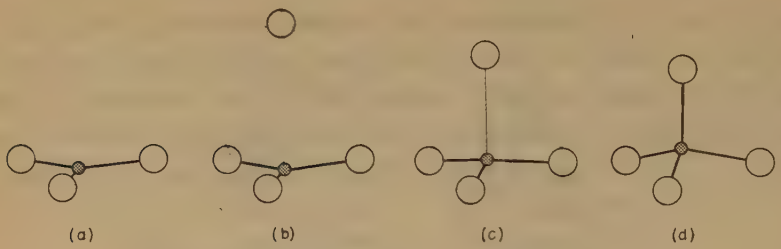

Fig. 13 Various coordinations of boron atoms.

Except separarte BO_3 groups in orthoborates, the coplanar BO_3 groups as a constituent element of a polyatomic ions also appear to have a tendency to form, with another oxygen atom, a very acute oxygen pyramid (Fig. 13 b). The distances between boron and the fourth oxygen atoms found in various borates are listed as follows.

Crystal	Distance between oxygen at the apex of acute pyramid and boron in the basal plane.
boric acid*[24]	3.157 Å 3.184
calcium metaborate[25]	3.10
borax[12]	2.99
suanite[18]	3.11
sodium metaborate[15]	3-23
potassium metaborate[21]	3.67
potassium acid dihydronium pentaborate[22]	3.83

* The structure of boric acid may be regarded as composed of H_3BO_3 sheets rather than of separte BO_3 groups.

It is interesting to note that, in such structures where the octahedral oxygen groups with metal atoms (say magnesium) inside form endless chain, the BO_3 groups and (B_2O_5) groups arrange themselves in different ways; e.g., in ludwigite, the planes of BO_3 groups are at right angle to the chains, while, in suanite, the effective planes of the (B_2O_5) groups are inclined to the chains so that an oxygen in one (B_2O_5) group forms an acute oxygen pyramid with a BO_3 group which is the constituent element of another (B_2O_5) group (Fig. 14).

Classification of borate polyatomic ions.

As shown in the previous paragraph, the classification of borate

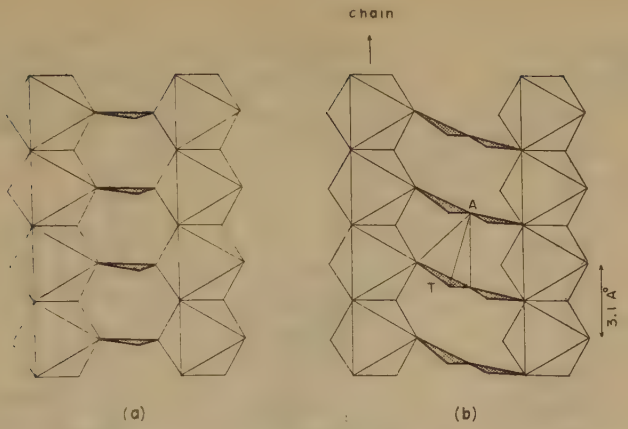

Fig. 14 Comparison of arrangement of BO_3 groups in ludwigite (a) and that of B_2O_5 groups in suanite (b) where one acute oxygen pyramid formed by oxygen, A, and triangle, T, is shown.

polyatomic ions may rest on the three structural types; i.e. types with triangular-, tetrahedral- and hybrid configurations. Another way of classification will be made on the bassis of the configurations of the polyatomic ions as a whole, and the types of the ions thus classified will be 'separate group', 'chain', 'network' and perhaps 'sheet'.

However, it is also possible to classify them by the number of constituent tetrahedra and triangles in the boron-oxygen groups or in the asymmetric unit of infinite groups. The borate polyatomic ions summarized in Table 4 are classified in these ways.

The (B_3O_6) chain, mono-tetrahedral di-triangular borate chain, is the one found in monoclinic metaboric acid, HBO_2[23]. This chain structure also presents an example which well supports the discussion on the nature of B-O bond as given above because the asymmetric unit of the chain consists of a (B_2O_5) group and a BO_4 tetrahedron. Although the detail account on the structure has not been reported, the chain structure may be schematically shown as given in Fig. 15 where it is compared with the other two borate chains.

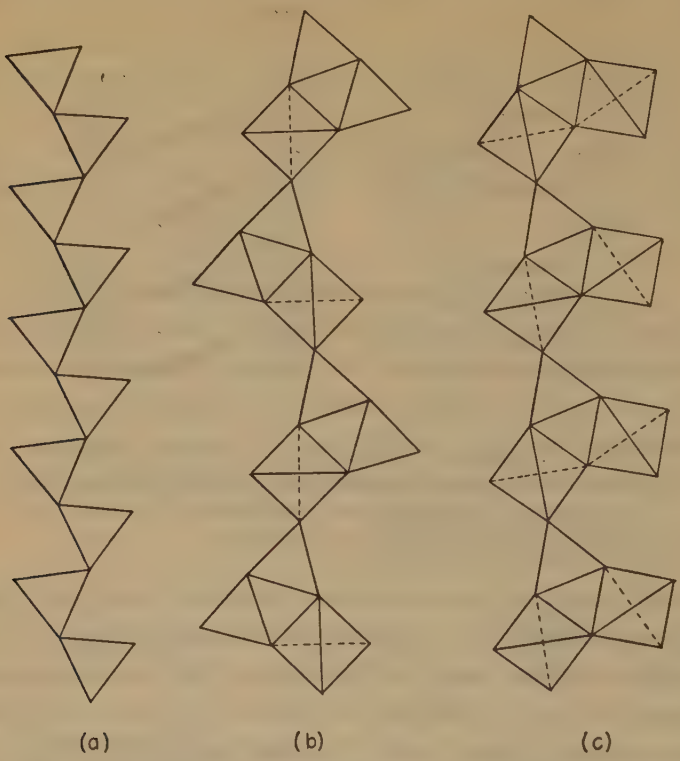

Fig. 15. A schematical presentation of boron-oxygen chains.
(a) B_2O_4 (b) B_3O_6 (c) B_3O_7

Table 4. Classification of borate polyatomic ions.

No. of tetrahedron	No. of triangle	Separate group	chain	network	sheet
0	1	BO_3 kotoite			*
	2	B_2O_5 suanite	B_2O_4 calcium metaborare		*
	3	B_3O_6 potassium metaborate			*
	4				*

	0	BO_4 teepleite			·|·
	1				·|· *
1	2		B_3O_6 metaboric acid		·|· *
	3				·|· *
	4	B_5O_{10} potassium acid dihydronium pentaborate			·|· *
	0	B_2O_7 pinnoite		B_2O_3 boron oxide	·|·
	1	B_3O_8 meyerhofferite	B_3O_7 colemanite		·|· *
2	2	B_4O_9 borax			·|· *
	3				·|· *
	0				·|·
3	1				·|· *
	2				·|· *
	0				·|·
4	1				·· *
5	0			B_3O_{12} boracite	··

* Triangular configuration.
·\|· Tetrahedral configuration.
·\|· * Hybrid configuration.

Acknowledgements

I am indebted to Professor T. Ito and Dr. R. Sadanaga for helpful

discussions. Special acknowledgement is due to Dr. K. Ichishima of the Chemical Institute for discussions and various facilities for the present experiments. Thanks are also due to Professor T. Watanabé for furnishing materials, to Professor R. Kiriyama, Osaka University, and to Mr. Y. Iitaka for valuable comments.

References

1) Berger, S.V.; Acta Chem. Scand., **7**, 611 (1953).
2) Berger, S.V.: Acta Chem. Scand., **4**, 1054 (1950).
3) Christ, C.L., Joan R. Clark and H.T. Evans JR ; Acta Cryst., **7**, 453, (1954).
4) Christ, C.L. and Joan R. Clark: Acta Cryst., **9**, 830, (1956).
5) Fornaseri, M.; Perio. Mineral., **18**, 103, (1949).
6) Frondel, C., V. Morgan and J.L.T. Waugh; Am. Mineral., **41**, 927, (1956).
7) Horning D.F. and R.C. Plumb; J. Chem. Phys., **26**, 637 (1957).
8) Hunt, J.M., M.P. Wisherd and L.C. Bonham; Anal. Chem. **22**, 1478, (1950).
9) Ito, T.; *X-Ray Studies on Polymorphism. Tokyo*: *Maruzen*, (1950).
10) Ito, T., N. Morimoto and R. Sadanaga: Acta Cryst., **4**, 310, (1951).
11) Miller, A.F. and C.H. Wilkins: Anal. Chem., **24**. 1253, (1952).
12) Morimoto, N.: Mineralogical Journal, **2**, 1. (1956).
13) Paton, F. and S.G.G. MacDonald,: Acta Cryst., **10**, 653, (1957).
14) Steele, W.C. and J.C. Decius: J. Chem. Phys., **25**, 1184, (1956).
15) Ssu-Mien Fang: Z. Krist., **99**, 1. (1938).
16) Takéuchi, Y.: Mineralogical Journal, **2**, 78, (1957).
17) ———; Acta Cryst., **3**, 208, (1950).
18) ———; Acta Cryst., **5**, 574, (1952).
19) ———. T. Ito ond T. Watanabé: Acta Cryst., **3**, 98, (1950).
20) ———; Mineralogical Journal, **2**, 19, (1956).
21) Zachariasen, W.H.: Chem. Phys., **5**, 919, (1937).
22) ———: Z. Krist., **98**, 266, (1937).
23) ———: Acta Cryst., **5**, 68, (1952).
24) ———; Acta Cryst., **7**, 305, (1954).
25) ———. and G.E. Ziegler: Z. Krist., **93**, 354, (1932).

Manuscript received April, 20, 1958.

Mineralogical Journal, Vol. 2, No. 4, pp. 269-278, June, 1958

ELLIPTIC VIBRATION OF LIGHT IN SOME ALKALI AMPHIBOLES*

Tokugoro Shoda

Mineralogical Institute, University of Tokyo

Arstract

Observations were made of the elliptic vibration of light in some alkali amphiboles which are anomalous in extinction, and the ellipticity of vibration in arfvedsonite and riebeckite were determined. The results here obtained are similar to those previously obtained for heikolite.

Introduction

Some alkali amphiboles, at least certain members with strong light absorption are known to fail in showing complete extinction between crossed nicols, even when observed with a monochromatic light. Most of the previous investigators[1),2),6)] attributed this anomalous property to the perthitic intergrowth or twins in the mineral. However, the present writer,[7),8),9)] from the results of his photometric experiment on heikolite,[4)] a variety of arfvedsonite,[5)] especially on its (010) section, has shown that the anomalous optical property of the mineral may be due to the elliptic vibration of light wave, casued by strong absorption of light.

In this paper it will be shown that the above conclusion holds good for other amphiboles anomalous in extinction, and that optical phenomena due to the elliptic vibration are observed in those amphiboles as in heikolite.

The ellipticity of the vibration in two members of alkali amphiboles, arfvedsonite and riebeckite, was determined.

---

* Read at the joint meeting of the Mineralogical Society of Japan, the Japanese Association of Mineralogists, Petrologists and Economic Geologists, and the society of Mining Geologists of Japan, held in Sapporo on Sept. 28, 1957.

Experimental

For determining the axial ratios and the orientations of the principal axes of two elliptic vibrations in each of the (010) sections of arfvedsonite and riebeckite, a microscope with three rotation stages was used.

A $\frac{1}{4}\lambda$ plate was placed on the lowest stage, another $\frac{1}{4}\lambda$ plate on the highest stage, and the section on the stage between the above two. The vibration direction Z′ of the upper $\frac{1}{4}\lambda$ plate was made parallel to X′ of the lower $\frac{1}{4}\lambda$ plate.

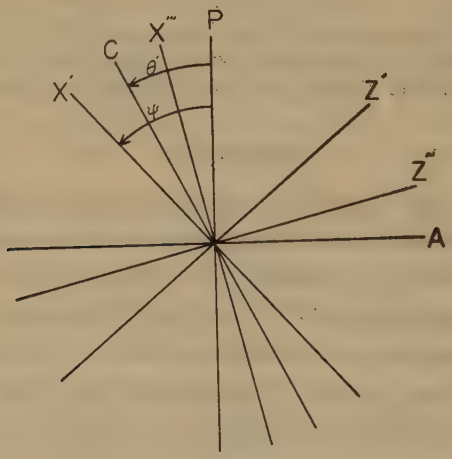

Fig. 1 Diagram showing the vibration directions X′, Z′ of the lower $\frac{1}{4}\lambda$ plate, that of ihe polarizer P, the analyzer A, the directions of the major axes of two elliptic vibrations X‴, Z‴ and the cleavage trace on the (010) section C.

The various optical directions above referred are shown in Fig. 1, in which ϕ denote the angle between the vibration direction of the polarizer and X′ of the lower $\lambda\frac{1}{4}$ plate, and θ' the angle between the cleavage trace in the section and the vibration direction of the polarizer.

A light of the wavelength of 587 mμ from the monochromator was used. The intensity of the transmitted light was measured by a photometer[3] which consists of a photomultiplier and a galvanometer. The

measurements were made on a relative scale.

Measurements on arfvedsonite

The specimen of arfvedsonite used in this experiment is one from Nunarsuatsiak, Tunugdliarfik in Greenland. A (010) section of this specimen placed between two $\frac{1}{4}\lambda$ plates was examined between crossed nicols, as to the ellipticity of vibration.

The variation in the intensity of light with rotation of the section was observed for a given ψ, which ranges from 0° to 180°. For each value of ψ, the values of the minimum intensity and the corresponding positions were determined. The results are shown in Figs. 2 and 3.

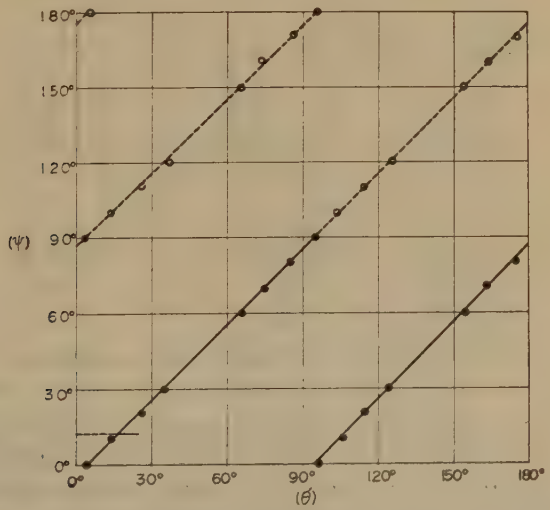

Fig. 2 Positions for the minimum intensity of light on the (010) section of arfvedsonite for various values of ψ (crossed nicols).

● and full lines: For the right handed incident light wave.
○ and broken lines: For the left handed incident light wave.

As is seen in Fig. 2, the points for minimum intensity approximately lie on two straight lines which make an angle of 45° to the abscissa, and the abscissa value of one line corresponding to a given

ordinate value differs from that of the other line by about 90°. Thus, the result here obtained for arfvedsonite is almost the same with that for heikolite[9] previously reported.

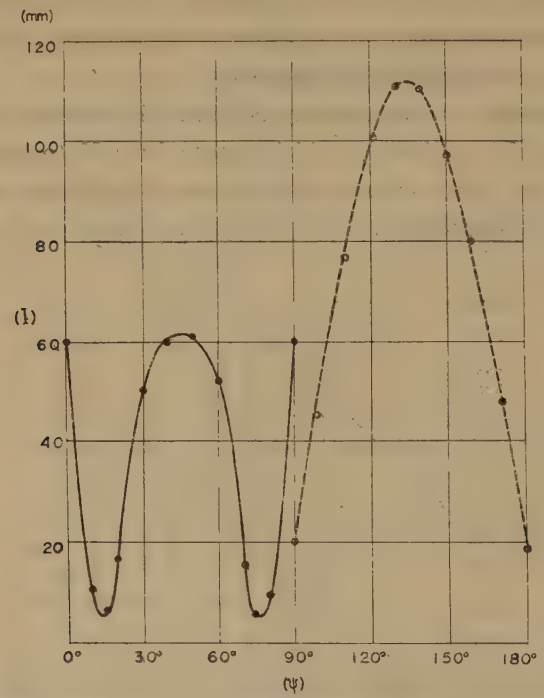

Fig. 3 The values of the minimum intensity on the (010) section of arfvedsonite for various values of ψ (crossed nicols).
● and full line: For the right handed incident light wave.
○ and broken line: For the left handed incident light wave.
I: Scale readings on the galvanometer.

Fig. 3 shows the relation between the minimum intensity and ψ. The intensity becomes nearly zero at the positions corresponding to $\psi=12°$ and $\psi=78°$. The value of axial ratio of the ellipse calculated by use of the equation $\tan\psi=\varepsilon$ is: $\varepsilon=+0.212$.

As was shown previously, the abscissa value θ' for a line in Fig. 2, corresponding to the ordinate value of 12°, gives the orientation of

X''' in the section. Here we obtain: $\theta'=16°$

From this we have: $CX'''=4°$

In order to examined whether the axial ratio and the orientation of the axes of elliptic vibration depend on the thickness of the section, similar measurements were made with the (010) section, considerably thicker than that used in the above experiment.

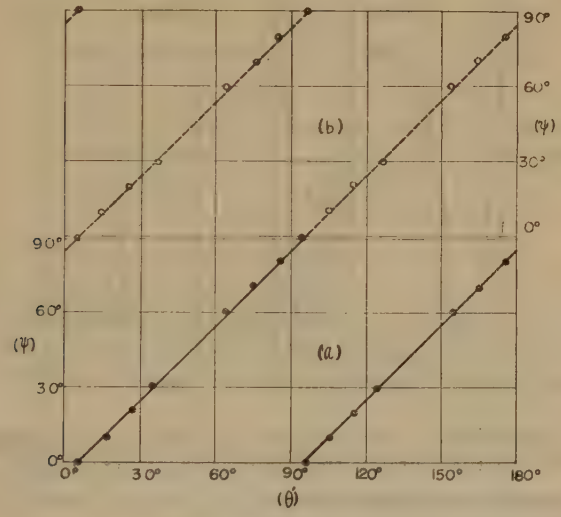

Fig. 4 Comparison of the positions for minimum intensity for the thinner section (a) with that for the thicker section (b) of arfvedsonite.

(a) Comparatively thin section.
(b) Comparatively thick section.

In Figs. 4 and 5, the result obtained for the thicker section is compared with that for the thinner. Only the data for $\phi=0°\sim90°$ are shown.

As is readily seen from the figures, the positions for the minimum intensity in Fig. 4 (a) are in good agreement with those in Fig. 4 (b), and the values of ϕ corresponding to the two minima of the curve in Fig. 5 (a) are approximately equal to those in Fig. 5 (b).

Therefore, as was assumed in the previous paper[9], no change occurs

in the axial ratios and the directions of the principal axes of the two elliptic vibrations, in the passage of a monochromatic light through the section.

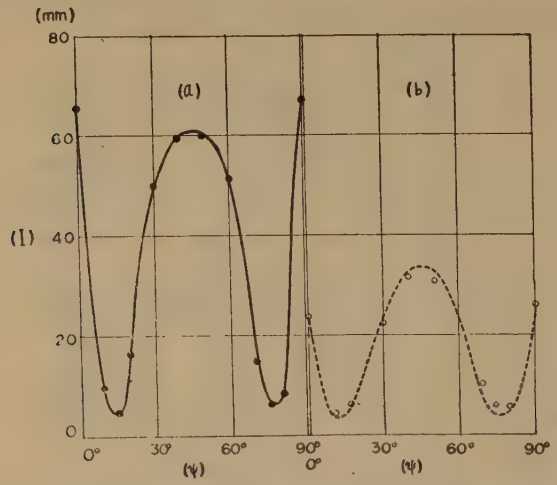

Fig. 5 Comparison of the I versus ϕ curve for the thinner section with that for the thicker section of arfvedsonite.
(a) Comparatively thin section.
(b) Comparatively thick section.

Measurements on riebeckite

The (010) section of riebeckite from St. Peter's Dome, El Paso County, Colorado was prepared. With this section, the optical observation was made in the same way as with the section of arfvedsonite, in order to determine the ellipticity af vibration.

The results are shown in Figs. 6 and 7. The minimum intensity becomes nearly zero at the values of $\phi=5°$ and $\phi=85°$ (Fig. 7). From this, the axial ratio of elliptic vibration in this section is given as: $\varepsilon=+0.087$ From the result shown in Fig. 6, the orientation of X''' is obtained as: $\theta'=11°$ and from this we have: $CX'''=6°$

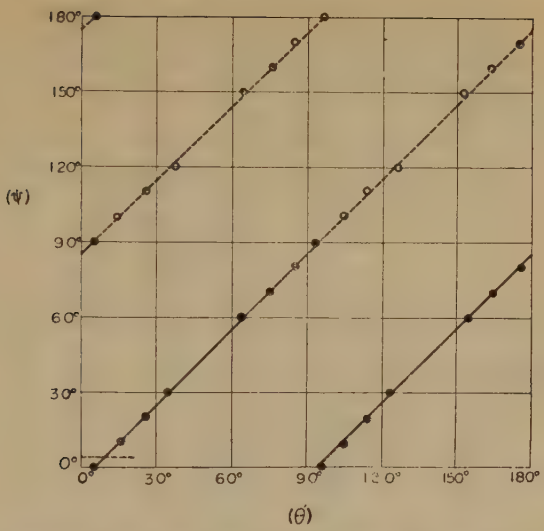

Fig. 6 Positions for the minimum intensity on the (010) section of riebeckite for various values of ϕ (crossed nicols).
● and full lines: For the right handed incidend light wave.
○ and broken lines: For the left handed incident light wave.

Comparison of the curves obtained for three amphiboles

In Fig. 8, the ϕ versus I curves for the two alkali amphiboles here treated (a and b) and for heikolite (c) are compared. For reference, a curve expected for a mineral normal in extinction (d) is also shown in the figure.

As is seen from Fig. 8, the form of the curve changes gradually from (a) to (d) as the axial ratio ε decreases. The intensity is much stronger for the left handed incident circular polarization ($\phi=135°$) than for the right handed ($\phi=45°$) in (a). This difference in intensity becomes smaller in (b), still smaller in (c), and finally becomes zero in (d).

From the result of the present experiment, it is inferred that there are various alkali amphiboles with different ellipticity in the vibration of the light passing through them, and that the abnomality in extinc-

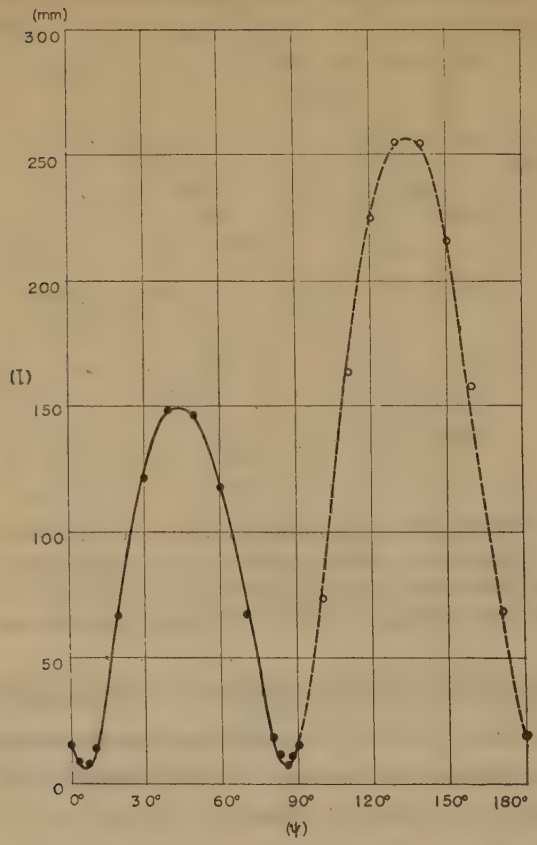

Fig. 7 The values of the minimum intensity on the (010) section of riebeckite for various values of ϕ (crossed nicols).
● and full line: For the right handed incident light wave.
○ and broken line: For the left handed incident light wave.

tion in them depend mainly on the ellipticity. So far as is known, heikolite is the largest in the value of ε and is the most remarkable in regard to the abnormality in extinction on (010) section.

Acknowledgements

The writer wishes to thank Professors. T. Ito and N. Katayama

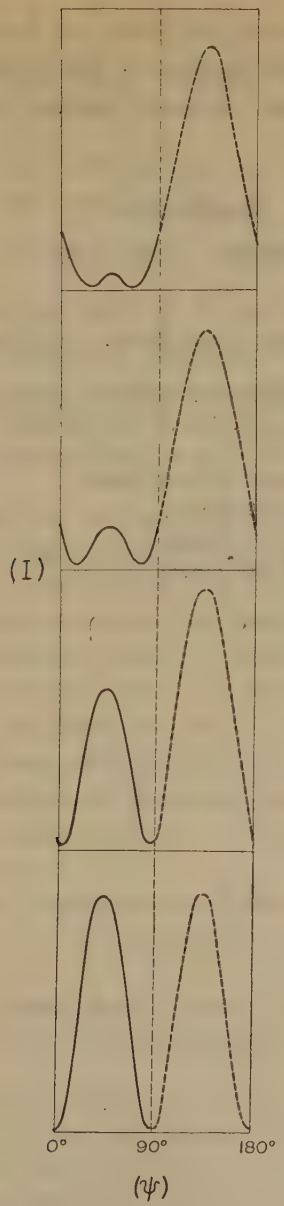

Fig. 8 Comparison of the form of ψ versus I curve.
Full lines: For the right handed incident light wave
Broken lines: For the left handed incident light wave

for their encouragement during this work. He is also indebted to Dr. A. Miyashiro who offered the specimen of arfvedsonite, and to Mr. T. Watanabe of the Earthquake Research Institute for preparation of sections.

References

1) Eskola, P. and T. S. Schahlstein: Bull. Comm. Geol. Finland, **92**, 89 (1930).
2) Hori, S.: Jour. Geol. Soc. Jap., **49**, 445 (1942) (in Japanese).
3) Katayama, N. and Y. Sato: Jour. Miner. Soc. Jap., **1**, 73 (1953) (in Japanese).
4) Kinosaki, Y.: Chosen-Kobutsushi, 198 (in Japanese).
5) Miyashiro, A.: Jour. Fac. Sc. Univ. Tokyo, Sect. 2 Vol. 11 Part. 1, 57~83 (1957).
6) Sahama, T. G.: Amer. Miner., **41**, 509 (1956).
7) Shoda, T.: Miner. Jour., **1**, 69 (1954).
8) Shoda, T.: Miner. Jour., **2**, 39 (1956).
9) Shoda, T.: Miner. Jour., **2**, 114 (1957).

Manuscript received April 25, 1958

ABSTRACT OF THE KOBUTSUGAKU ZASSHI,

JOURNAL OF THE MINERALOGICAL SOCIETY OF JAPAN, VOL. 3, NO. 5,

February, 1958

On the Iron Distribution in Rhodochrosite from the Imai-Isizaki Mine, Hokkaido (pp. 369-380)

Zyunpéi Harada and Yu Hariya

X-ray fluorescence analyses have been developed for the determination of the variation of Fe-content and for the confirmation of the presence of siderite component in rhodochrosite from the Imai-Isizaki mine, Hokkaido.

The analytical results indicated that Fe-content varies from depth of the ore bodies and also from stage of mineralization. We ascertained the presence of siderite, $FeCO_3$, crystals in rhodochrosite, comparing with mechanical mixture of $MnCO_3$ and $FeCO_3$. Therefore, we came to the conclusion that in rhodochrosite from the Imai-Isizaki mine, Fe may occur partly as siderite, mixing with rhodochrosite mechanically and partly as isomorphous mixed crystals, in which Fe replaces Mn in rhodochrosite.

Sepiolite from Yoshikawa-mura, Fukuoka Prefecture, Japan (pp. 381-387)

Hisashi Muraoka, Hideo Minato, Yukio Takano and Yôhachiro Okamato

Sepiolite ($6SiO_2 \cdot 4MgO \cdot 2H_2O$?) occurred from Dondon, Wakita, Yoshikawa-mura, as an altered material of serpentine in Sasaguri district. It is white colour and shows wax like appearance and fiber texture; hardness is 2-25, and indices of refraction are $Ng = 1.528$ and $N_p = 1.518$: its chemical analysis follows: SiO_2 49.42, TiO_2 none, Al_2O_3 trace, Fe_2O_3 0.03, FeO 0.42, NiO 0.06, MnO none, MgO 22.03, CaO trace, $Na_2O + K_2O$ 0.12, $H_2O(+)$

9.99, $H_2O(-)$ 18.49, total 100.56% (analysed by H. Muraoka in 1950). X-ray powder pattern of the specimen agrees with that from Morabia, New Mexico and Ampandrandava, and D.T.A. method has been carried out and an endothermic peak in 440°C is not observed on that specimen. Further X-ray investigation and thermal experiment must be succeeded to this report. It is the first occurrence of sepiolite in Japan.

Kaolin Minerals in "Roseki" (pp. 388–405)

Hideo Takeshi

In Japan, there are many roseki deposits, the ores of which consist mainly of pyrophyllite, kaolin minerals and diaspore. They are formed from the alteration of eruptive igneous rocks.

The following minerals are recognized as belonging to the kaolin group: nacrite, dickite, kaolinite, 'fireclay', dehydrated halloysite.

The writer studied kaolin minerals in many important roseki deposits of this country and found nacrite, dickite, 'fireclay' and kaolinite.

Nacrite and dickite are found mainly associated with diaspore at the central zone of the deposits. Kaolinite and 'fireclay', on the contrary, are found mainly associated with pyrophyllite at the outer zone of the deposits.

Lenticular masses which are composed of dickite are found in pyrophyllite zone or between pyrophyllite zone and alunite zone at Shokozan roseki deposit, Hiroshima Prefecture. The crystallinity of it is relatively lower than that of dickite which is born in diaspore ores. In some roseki deposits the writer found 'fireclay' type kaolin, the X-ray diffraction pattern of which is distinctive from that of kaolinite of low crystallinity which are found at some roseki deposits.

A Thermodynamic Study of Equilibrium Relations among Some Manganese Minerals Introduced during the Epoch of Thermal Metamorphism (pp. 406 417)

Mayumi Yoshinaga

As an aid to solve problems of mineral paragenesis concerning contact-metamorphosed manganese ore deposits, P-T equilibrium relations are

calculated, applying known thermodynamic data, for the following four reactions:

(a) $MnCO_3 = MnO + CO_2$

(b) $MnCO_3 + SiO_2 = MnSiO_3 + CO_2$

(c) $2MnCO_3 + SiO_2 = Mn_2SiO_4 + 2CO_2$

(d) $MnCO_3 + MnSiO_3 = Mn_2SiO_4 + CO_2$

Some of the results are important for the understanding of metamorphism in nature, particularly under the action of heat effects. At high temperatures, the reaction is shifted in favour of manganosite. At lower temperatures, under any pressure conditions up to 5000 atm., tephroite is thermodynamically more stable than rhodonite.

Optical Anomaly of Analcime from Mazé, Niigata Prefecture

(pp. 418-423)

Ryôiti Kiriyama and Masaaki Azumi

The amount of the double refraction of the transparent, icositetrahedral crystal of analcime from Mazé was measured by a Berek compensator. The value was about 0.0003. The lattice constant was determined as a= 13.70 Å assuming a cubic lattice.

There was no change of the double refraction in the long run after several hours' treatment of setting the specimen in a stream of water vapour at normal atmospheric pressure.

The result of the heating experiment was that the amount of the double refraction increased up to 0.001 for 4 hours heating at 300°C. and the lattice was also distorted from the ordinary, pseudocubic one to a presumably tetrahedral one with a=13.70 Å and c=13.55 Å. Higher the temperature of such a treatment, larger the optical anisotropy and the lattice distortion was observed distinctly.

It is concluded that the lattice of analcime must have been formed with a cubic symmetry under a certain hydrothermal condition, as the temperature is cooled down, the lattice gradually becomes distorted as the result of a little amount of bending of the bond angles, O-Si-O or O-Al-O in the three-dimensional framework of the original lattice, then the slightly distorted cubic lattice may cause its optical character to be anisotropic.

Communications on Minerals of Japan (Part 12)

(pp. 424-433)

Mumeikai Group

30. *Voltaite from the Yanahara Mine, Okayama Prefecture*

Nagashi Ogushi, Akira Kato, Kin-ichi Sakurai and Yukio Sakamaki

Voltaite was found in the third level, No. 1 ore body, Yanahara mine, Okayama prefecture.

It occurs associated with alunogen. The crystal attaining about 2mm in size displays good faces of *o*(111), *a*(100) and *d*(110).

It was identified by the crystal form, x-ray powder data, qnalitative analyses and refractive index.

31. *Szomolnokite and Mirabilite from the Yanahara Mine, Okayama Prefecture*

Nagashi Ogushi and Akira Kato

Szomolnokite and mirabilite were found in No. 1 ore body, Yanahara mine, Okayama prefecture.

The former occurs in thin, dark brown crust on a fissure of the country rock and the latter associated with melanterite.

They were identified by x-ray powder data and qualitative analyses.

32. *Hübnerite from the Kaso Mine, Tochigi prefecture*

Akira Kato

Hübnerite was found in the Kaso mine, Tochigi prefecture. It occurs in platy crystal enclosed in Mn ore mainly composed of rhodonite.

The identification was based on the x-ray powder data.

Hübnerite of such occurrence may be a product in contact metamorphosed manganese deposits by granitic rocks as like as scheelite in calcium carbonate rocks.

Reviews

Infra-red Absorption of Minerals.....Ryôiti Kiriyama 434-450

Proceedings.....455

Mineralogical Society of Japan

OFFICERS FOR 1958–1959

President: Teiichi Ito, University of Tokyo, Tokyo.

Vice-President: Bumpei Yoshiki, Asahi Glass Co. Ltd., Tokyo.

Secretary: Toshio Sudo, Tokyo University of Education, Tokyo. Keiichi Omori, Tohoku University, Sendai.

Treasurer: Tokugoro Shoda, University of Tokyo, Tokyo.

Editor: Nobuo Katayama, University of Tokyo, Tokyo.

Councillors: Zyunpéi Harada; Hokkaido University, Sapporo. Keiichi Omori, Tsunehiko Takeuchi; Tohoku University, Sendai. Shuichi Iwao, Nobuo Katayama, Eiichi Minami, Hideo Minato, Ryoichi Sadanaga, Tokugoro Shoda, Seitaro Tsuboi, Takeo Watanabe; University of Tokyo, Tokyo. Toshio Sudo, Tokyo University of Education, Tokyo. Teiroku Sueno, Onoda Cement Co. Ltd., Tokyo. Ichiro Sunagawa, Geological Survey of Japan, Tokyo. Kin-ichi Sakurai, Tokyo. Ryoiti Kiriyama, University of Osaka, Osaka. Kitinosuke Henmi, Okayama University, Okayama. Yoshio Kinosaki, Hiroshima University, Hiroshima. Kameki Kinoshita, Toyofumi Yoshimura; Kyushu University, Fukuoka.

PUBLICATIONS

Kôbutsugaku Zasshi, Journal of the Mineralogical Society of Japan

A journal containing articles and reviews on mineralogy and allied sciences contributed by members of the Mineralogical Society of Japan. Published every four months, in Japanese. Sent to all members of the Society. Membership dues $2.00 annually.

Mineralogical Journal

A journal containing articles on mineralogy and allied sciences, published semi-annually in English principally. Contributions are invited from everyone. The Journal completed its first volume of six numbers in 1956. Back numbers may be obtained at $1.00 per single copy for the time being. The price of subscription to the second volume is $5.00 per volume.

Printed by "HERALD" Printing Co., Ltd.